THE EUROPEAN SOCIETY OF MEDICINE
Medical Research Archives, Volume 14 Issue 3

RESEARCH ARTICLE

Single-cell RNA sequencing analysis reveals MDK/SDC4-dependent anti-PD1 treatment tolerance in endometrial cancer

Muturi Njoka[1], Yanming Li[2] and Stefan H. Bossmann[1*]

[1]Department of Cancer Biology, University of Kansas Medical Center, Kansas City, KS, USA
[2]Department of Biostatistics & Data Science, University of Kansas Medical Center, Kansas City, KS, USA

[*]sbossmann@kumc.edu

OPEN ACCESS

PUBLISHED
31 March 2026

CITATION
Njoka, M., Li Y. and Bossmann, SH., 2026. Single-cell RNA sequencing analysis reveals MDK/SDC4-dependent anti-PD1 treatment tolerance in endometrial cancer. Medical Research Archives, [online] 14(3).

ISSN
2375-1924

ABSTRACT

Background: Endometrial cancer (EC) is the most common gynecological malignancy in developed countries. The antibodies targeting the programmed death 1 (PD-1) pathway (anti-PD therapy) have transformed cancer treatment, including EC. However, only a fraction of EC patients respond to anti-PD therapy. The underlying mechanism leading to failure in other patients is less understood.

Methods: We performed single-cell RNA sequencing data analysis of an anti-PD1 responder and non-responder EC cases. Also, we analyzed spatial transcriptomics data of an endometrial adenocarcinoma case to determine cell colocalization. The Cancer Genome Atlas Uterine Corpus Endometrial Carcinoma (TCGA-UCEC) dataset was utilized to investigate the relationship between identified gene signatures and clinical outcomes. The analysis was done using the R software.

Results: The cells were classified into ten clusters with different pathways enriched between the anti-PD1 therapy responder and non-responder. The differentially expressed genes in these pathways accurately predicted the anti-PD1 therapy response in the single-cell RNA-seq data. Cell-cell communication revealed high signaling between the epithelial cells, mesangial cells, and regulatory T cells (Tregs). We discovered syndecan-4 (SDC4) as the Treg receptor for midkine (MDK/MK) associated with anti-PD1 therapy tolerance in EC. The epithelial cells were the major source of MDK, and they colocalized with the Tregs. Finally, the TCGA UCEC dataset analysis indicated that high expression levels of SDC4 correlated with poor overall survival in patients.

Conclusion: The single-cell RNA-seq analysis performed herein revealed MDK-SDC4 signaling as the driver inducing the immune suppression phenotype in the anti-PD1 therapy non-responder. These findings suggest that blocking the MDK-SDC4 signal might help to overcome the anti-PD1 therapy tolerance in EC. These results show novel potential immunotherapeutic targets in EC.

Keywords: endometrial cancer, anti-PD1 tolerance, single-cell RNA sequencing, midkine, syndecan-4.

Introduction

Endometrial cancer (EC) is the most common gynecological malignancy in developed countries[1]. There are two major types of uterine cancer: sarcomas, which emerge in the muscular myometrium layer, and adenocarcinomas, ~80% of total cases, arising from the endometrium[2]. The high disease-free survival rate is attributed to both the early detection of EC and the effectiveness of surgery in treating early-stage/low-grade EC. However, poor outcomes are associated with high-grade, metastatic, or recurrent disease, which is on the rise[3].

Endometrial cancer has high inter- and intra-tumoral heterogeneity[4], which plays a critical role in tumor treatment response and progression[5]. Although cancer is caused by genetic mutations, different tumor cell clones are surrounded by immune cells and stromal cells, referred to as the tumor microenvironment (TME)[6]. TME diversity includes tumor-associated macrophages (TAMs), immune tolerance-related cells, and cancer-associated fibroblasts (CAFs), which influence response to anti-cancer therapy[7]. Therefore, identifying critical cell–cell interactions and the genes involved in crosstalk in the TME is imperative.

Immunotherapy using antibodies targeting the programmed death (PD1) receptor pathway (anti-PD1 therapy) has revolutionized cancer treatment. The anti-PD1 therapy uses monoclonal antibodies that target the immunosuppressive TME by blocking the immune inhibitory receptor PD-1 and its ligand B7-H1 (also known as PD-L1)[8]. However, the response of patients with EC to anti-PD-1 PD-1 inhibitors, like pembrolizumab and nivolumab, varies[9]. The reason for failure in some patients is less known. Understanding the immune tolerance in TME at the single-cell level resolution may provide a better understanding of the differences between treatment outcomes[10]. Single-cell RNA sequencing (single-cell RNA-seq) measures gene expression levels for thousands to millions of individual cells and deconvolutes heterogeneity at the cellular level[11]. Recent advances in single-cell RNA-seq technology have identified key immune cells associated with the response to anti-PD therapy[12–14].

In this study, we integrated the single-cell RNA-seq data from Gene Expression Omnibus (GEO, accession code GSE251923), with Molecular Signatures Database (MSigDB) data. We identified this as the only single-cell RNA-seq data in the GEO database that compared the anti-PD1 responders to non-responders by July 2025. The spatial transcriptomics (ST) data for endometrial adenocarcinoma tumor were downloaded from the 10x genomics database (accessed July 2025)[15]. The analysis dissected the mechanisms underlying immune tolerance and identified specific immune cell populations that might augment sensitivity to anti-PD-1 therapy in EC. We identified midkine MDK/SDC4 as the signaling pathway that induces Tregs in the EC anti-PD1 treatment failure. Epithelial cells and other cells send the MDK factor that signals through SDC4 on Tregs to promote an immunosuppressive TME. Single-cell RNA-seq and ST-seq data integration revealed epithelial cells colocalized with Tregs in the TME. Here, we report the possible mechanism of acquiring anti-PD1 therapy tolerance in endometrial cancer patients.

Material and Methods

STUDY DESIGN

In this study, we analyzed scRNA-seq data from two EC patient tumor tissues in GEO (GSE251923). We performed differential gene expression (DGE) and predicted the anti-PD1 treatment tolerance using Receiver Operating Characteristic (ROC) curve analyses. To validate the key findings of the identified differentially expressed genes, we estimated the patient survival between expression levels above and below the median. We performed cell-cell communication analysis using CellChat package (version 2.2.0)[16] to identify intercellular interaction drug target molecules. Finally, we determined cell colocalization using the ST-seq dataset.

DATA ACQUISITION

A published single-cell RNA sequencing data accessible in the GEO database with accession code GSE251923 was used[17]. The data was generated from two patients: Case A: responder to anti-PD-1 therapy; and Case B : non-responder to anti-PD-1 therapy. The TCGA UCEC project data (https://portal.gdc.cancer.gov, accessed July 2025) were used to validate the association between detected gene signatures and patient-level clinical significance.

SINGLE-CELL RNA TRANSCRIPT ANALYSIS

The R software (version 4.5.0) was used to analyze the single-cell RNA-seq data using the Seurat

package (version 5.3.0)[18]. Cells were filtered to retain the ones with more than 400 genes expressed, less than 25% unique molecular identifiers (UMIs) from the mitochondrial genome, and genes expressed in more than three cells. The hemoglobin and mitochondrial genes were removed from the data. The ribosomal genes were previously removed[17]. The data used for downstream analysis contained 18,082 transcripts for 17,593 cells.

The 'Harmony' function in Seurat was used to remove the batch effects, and the 'Find Variable Features' function identified highly variable genes. We performed the Z-score normalization followed by principal component analysis (PCA) with the highly variable genes. The top 15 significant principal components (PCs) were used to perform uniform manifold approximation and projection (UMAP) dimension reduction. The clusters were determined using the 'FindNeighbors' and 'FindClusters' functions using resolution 1. The cell type annotation was performed with the SingleR package (version 2.10.0)[19] using Blue Print[20] and Encode[21], reference cell type panels. Differentially expressed (DE) genes were determined using the 'FindMarkers' function in the Seurat package using the Wilcoxon rank sum test.

PREDICTING ANTI-PD1 THERAPY TOLERANCE USING MACHINE LEARNING

The DE genes data was divided into training data (14,193 cells) and the test data (1,700 cells), and the most variable genes were extracted using the SingleR package. We used 8 different machine learning (ML) methods in predicting the anti-PD1 tolerance, which include least absolute shrinkage and selection operator (LASSO) regression[22] using glmnet R package (version 4.1-10), ridge regression[23], elastic net (Enet)[24], Xgboost (version 1.7.11.1)[25], Linear discriminant analysis (LDA, version 7.3-65)[26], neural network (NN)[27], random forest using random Forest R package (version 4.7-1.6)[28], classification trees using part R package (version 4.1.24)[29]. The R package caret (version 7.0-1) was used to create confusion matrix and the ROCR package (version 1.0-11) calculated the overall performance (Area Under Curve (AUC) of the ML methods used.

PATHWAY ENRICHMENT ANALYSIS

The gene set enrichment analysis (GSEA) plus Gene Ontology (GO) was performed to compare the DE genes with the Kyoto Encyclopedia of Genes and Genomes (KEGG) gene pathways (Subramanian et al., 2007) available at Molecular Signatures Data Base (MSigDB)[30] using fgsea package (version 1.34.0). Pseudo bulk DE analysis was performed with DESeq2 package (version 1.48.1)[31]. The significantly enriched KEGG pathways were depicted using the ggplot2 package (version 3.5.2), showing significantly positively and negatively enriched pathways. For the gene set variation analysis (GSVA), msigdbr package (version 25.1.1) was used to retrieve human gene sets from 50 hallmark pathways. The pathway activity estimates were assigned to individual cells with GSVA package (version 2.2.0)[32].

THE CANCER GENOME ATLAS DATA ANALYSIS

The RNA sequencing data (transcripts per million, TPM), clinical data, and metadata for 499 UCEC patients were fetched from the TCGA database (https://portal.gdc.cancer.gov). The dataset had a total of 60,660 genes. The samples with incomplete clinical messages were manually cleaned. The survival analysis was conducted using the suvminer and survival R packages (version 3.8-3), and the curves were drawn with the ggplot2 package (version 3.5.2). Additional online survival analysis of the TCGA data was done using KMplot platform[33]. The ESTIMATES score was calculated using the Wilcoxon test in R software.

CELL-CELL COMMUNICATION ANALYSIS

We inferred the intercellular communications using CellChat package (version 2.2.0)[16] for single-cell RNA-seq data. This builds cell-cell communication atlases and discovers novel intercellular communications.

INTEGRATING SINGLE-CELL RNA-SEQUENCING DATA WITH SPATIAL TRANSCRIPTOMICS-SEQUENCING DATA

The Seurat R package was used for this integration analysis. The ST-seq data were normalized using log2 transformation, and dimensionality reduction was done by UMAP using the first 10 PCs. Cell type deconvolution analysis was done by predicting the single-cell RNA-seq cell type markers onto the ST-seq data. The data was visualized using the 'Spatial Feature Plot' function in Seurat. Spatial cell type proportions (cell colocalization) were visualized using ggplot2 R package.

Results

THERE WERE IMMUNE AND NON-IMMUNE CELL TYPES FROM ANTI-PD1 NON-RESPONDER AND RESPONDER

The cells were from the two EC patients treated with anti-PD1 Pembrolizumab 200 mg intravenously in combination with a pan-kinase inhibitor Lenvatinib 20 mg orally. There was a progressive disease in the Case B patient, and we treated it as an anti-PD1 non-responder. There was a partial response in the Case A patient, and we treated it as an anti-PD1 responder. We assessed the quality of the RNA sequencing platform by examining total gene counts per cell (Figure 1, a, Supplemental Figure 1, a). We filtered cells with more than 25% mitochondrial genes, less than 3% ribosomal genes, or more than 1% hemoglobin genes (Supplemental Figure 1, b). The batch effect between samples was removed using harmony integration and visualized using the UMAP (Figure 1, b). The cells were clustered using the Louvain algorithm (Figure 1, c). The cells were annotated using the marker gene expression in the Blueprint Encode Data (BPED) cell library and singleR package (Figure 1, d).

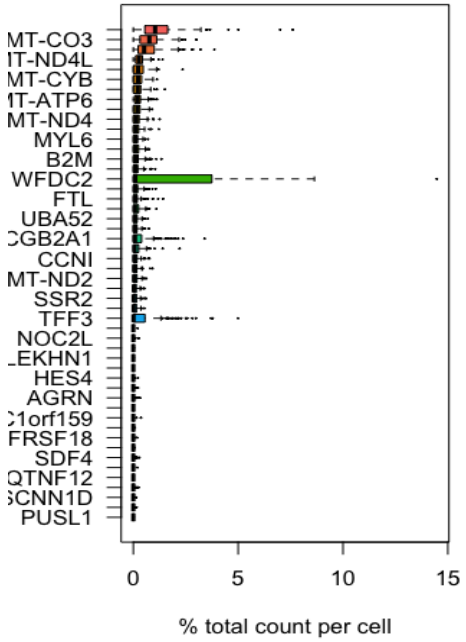

(a)

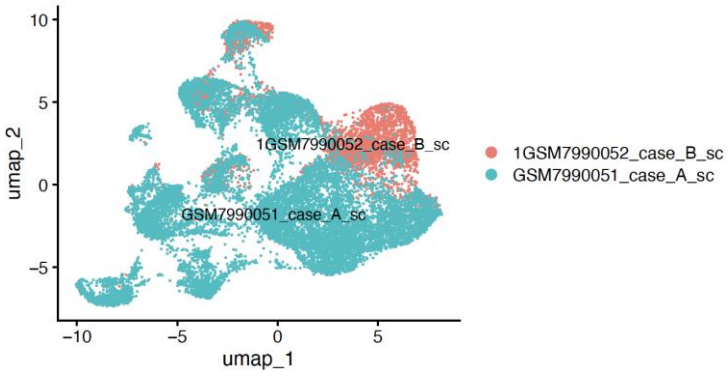

(b)

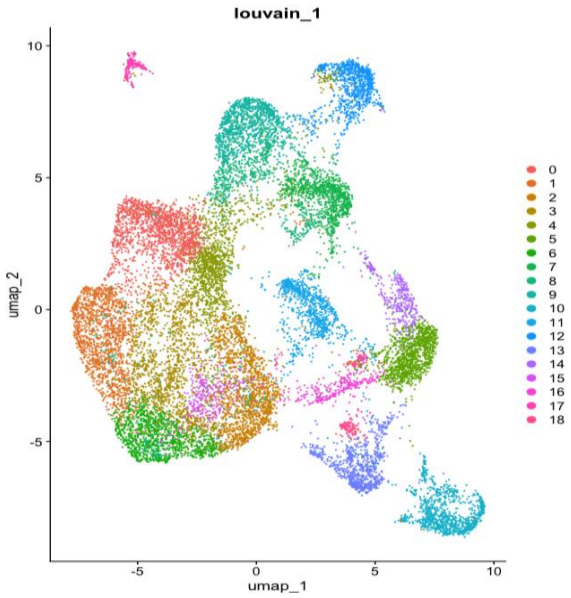

(c)

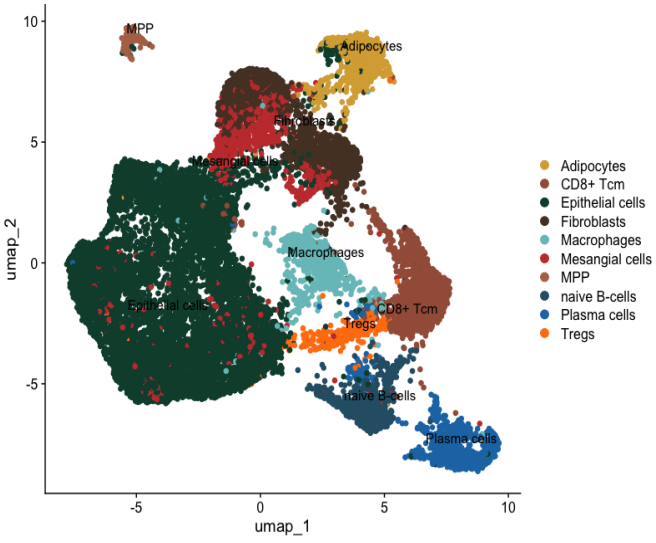

(d)

Figure 1. Immune and non-immune cell types from anti-PD1 non-responder and responder: (**a**) Box plot showing the mRNA quality per cell; (**b**) The Uniform Manifold Approximation and Projection (UMAP) showing the samples batch effect reduction after harmony integration of the cells; (**c**) UMAP showing 19 cell clusters; (**d**) UMAP showing cell clusters annotated into ten cell types.

ENRICHED PATHWAYS WERE IN BOTH IMMUNE AND NON-IMMUNE CELL TYPES

To identify genes or pathways that show significant expression changes between anti-PD1 responder and non-responder, we run the Gene Ontology (GO) and the Kyoto Encyclopedia of Genes and Genomes (KEGG) pathway analysis and select the three top GO terms by cell type (Figure 2, a). To get the sample-specific gene set analysis, we run GSVA analysis (Figure 2, b). To validate the single-cell RNA-seq differentially expressed (DE) gene analysis, we run the pseudo bulk DE gene analysis (Figure 2, c), followed by KEGG pathway analysis (Figure 2, d, e).

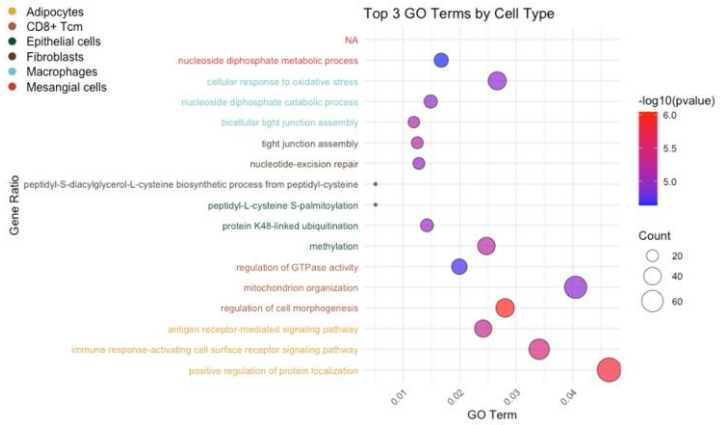

(a)

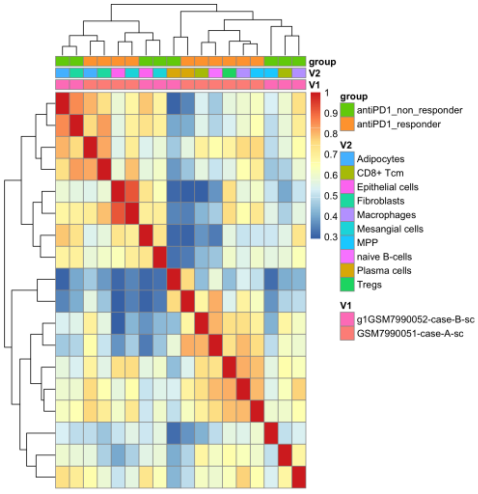

(b)

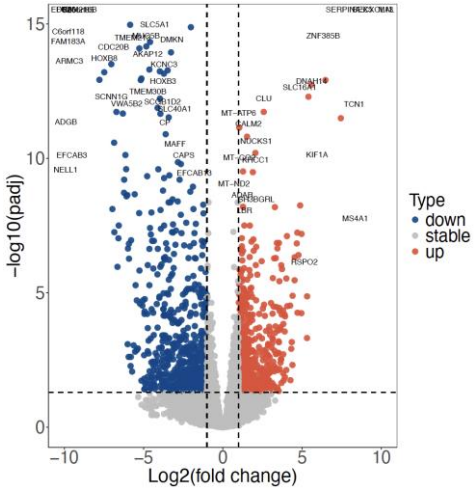

(c)

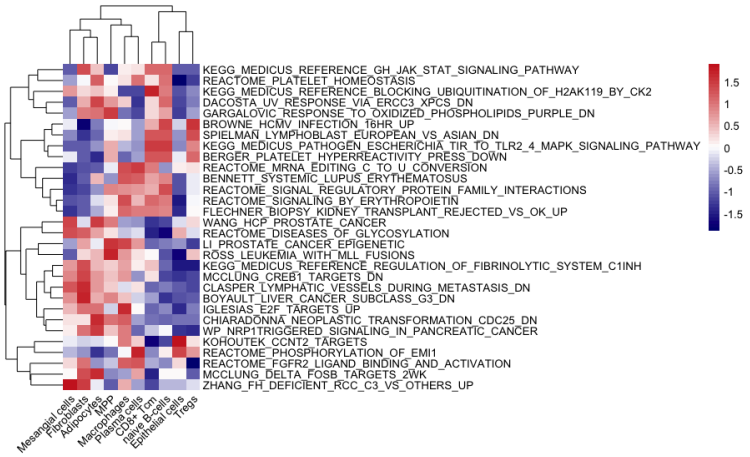

(d)

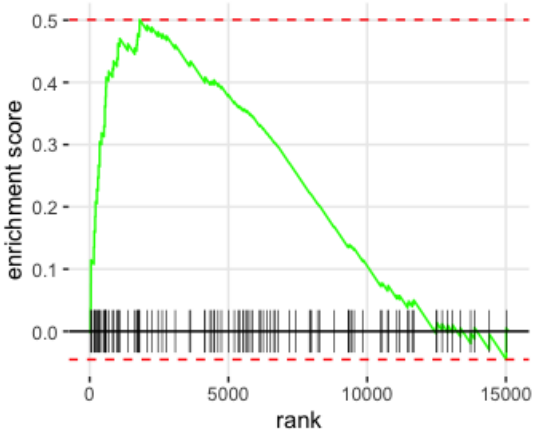

(e)

Figure 2. GO and KEGG show distinct enriched pathways among cell types: (**a**) Bubble plot showing the top three KEGG pathways enriched in individual cell types after GO enrichment analysis; (**b**) Heat map showing the individual cell types DEGs correlation between the anti-PD1 non-responder and responder after pseudo bulk analysis; (**c**) Volcano plot showing the DE genes after pseudo bulk analysis using DESeq2 R package; (**d**) Heat map showing the top 30 differentially expressed pathways in the anti-PD1 non-responder cells (KEGG or MSigDB); (**e**) Enrichment score plot for the top GSEA pathway (KEGG_T_CELL_RECEPTOR_ SIGNALING_ PATHWAY).

DIFFERENTIALLY EXPRESSED GENES PREDICTED THE ENDOMETRIAL CANCER PATIENTS' ANTI-PD1 TREATMENT OUTCOME AND SURVIVAL IN THE TCGA UCEC DATASET

To test the utility of DE genes in predicting the anti-PD1 treatment outcome, we evaluated the prediction scores of eight machine learning (ML) methods with cell types annotated in four cell libraries (BPED, Human Primary Cell Atlas Data (hpca), Database Immune Cell Expression Data (Immu), Novershtern Hematopoietic Data (nhd) (Table 1).

Table 1. The anti-PD1 therapy tolerance prediction scores using the BPED SingleR library

ML Model	ROC Score
LASSO	0.9989765
RIDGE	0.9981588
ENet	0.9987707
xgboost	0.9907718
Linear discriminant analysis (LDA)	0.94665
Neural network	0.9995995
Random forest	0.9440273
Classification trees	0.9322486

Among the top ten DE genes with a p-adjusted value < 2.2 X 10-16 were listed (Table 2).

Table 2. The top ten upregulated and downregulated DE genes

Top Up Regulated Genes							
Gene Symbol	**Description**	**Locus**	**avg_ log2FC**	**p_val _adj**	**Type of Cancer †**	**Immunosu ppression**	**Reference**
SLPI	Secretory Leukocyte Peptidase Inhibitor	20q13.12	5.98	0	PDAC, OvCa,	Yes	[34,35]
AKAP12	A-Kinase Anchoring Protein 12	6q25.1	8.10	0	N/A	N/A	N/A
SLC40A1	Solute Carrier Family 40 Member 1	2q32.2	5.23	0	CRC	Yes	[36]
TFF3	Trefoil Factor 3	21q22.3	3.90	0	EC	No	[37]
SCGB1D2	Secretoglobin Family 1D Member 2	11q12.3	4.57	0	BC	N/A	[38]
WFDC2	WAP Four-Disulfide Core Domain 2	20q13.12	5.51	0	N/A	N/A	N/A
ASRGL1	Asparaginase And Isoaspartyl Peptidase 1	11q12.3	3.34	0	RCC, CRC,	Yes	[39,40]
CHGA	Chromogranin A	14q32.12	8.56	0	lymphoma	Yes	[41]
F3	Coagulation Factor III, Tissue Factor	1p21.3	4.54	0	N/A	N/A	N/A
SCGB2A1	Secretoglobin Family 2A Member 1	11q12.3	2.86	0	BC	N/A	[38]
Top Down Regulated Genes							
Gene Symbol	**Description**	**Locus**	**avg_ log2FC**	**p_val _adj**	**Type of Cancer †**	**Immunosu ppression**	**Reference**
NUCKS1	Nuclear Casein Kinase And Cyclin Dependent Kinase Substrate 1	1q32.1	-2.88	0	Osteosarcom a, BC	Yes	[42,43]
CLU	Clusterin	8p21.1	-3.52	0	CRC	NA	[44]
SERPNA5	Serpin Family A Member 5	14q32.13	-7.72	0	BC,	No	[45,46]
IVNS1ABP	Influenza Virus NS1A Binding Protein	1q25.3	-2.30	0	HCC	No	[47,48]
SLC16A1	Solute Carrier Family 16 Member 1	1p13.2	-6.66	0	OvCa, RCC, UCEC	No	[49]
SRP9	Signal Recognition Particle 9	1q42.12	-1.74	0	BC	No	[50]
TXNIP	Thioredoxin Interacting Protein	1q21.1	-1.86	0	Melanoma	Yes (anti-PD1)	[51]
IGKC	Immunoglobulin Kappa Constant	2p11.2	-3.36	0	BC	No	[52]
IGHG1	Immunoglobulin Heavy Constant Gamma 1 (G1m Marker)	14q32.33	-5.02	0	BCa, CRC	No (anti-PDL1)	[53,54]
PSAT1	Phosphoserine Aminotransferase 1	9q21.2	-4.88	2.2e-309	BC	No (anti-PD1)	[55]

† hepatocellular carcinoma (HCC), breast cancer (BC), colorectal cancer (CRC), prostate cancer (PCa), pancreatic ductal adenocarcinoma (PDAC), ovarian cancer (OvCa), endometrial carcinoma (EC), not applicable (N/A), Renal cell carcinoma (RCC), bladder cancer (BCa).

Supplemental Figure 3, a - j). To assess the therapeutic target potential of the DE genes, we compared the gene expression between the EC tumors, endometrial adenocarcinoma (EAC), n = 374, Serous cystadenocarcinoma (SCC), n = 125, and adjacent normal tissues (EM), n = 35, in the TCGA UCEC dataset (Figure3, l; Supplemental Figure 3, k).

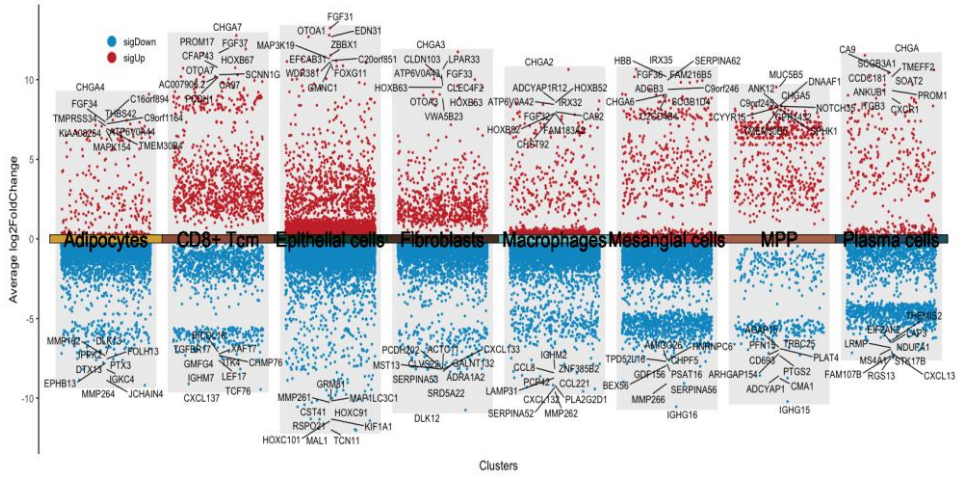

(a)

AKAP12

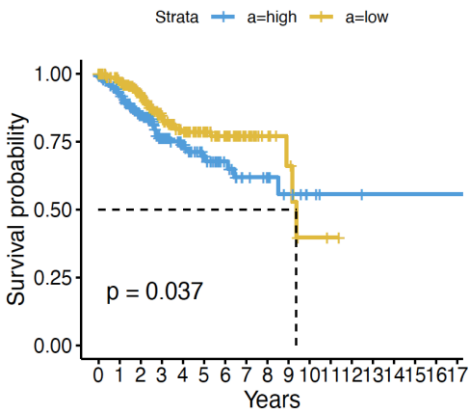

(b)

ASRGL1

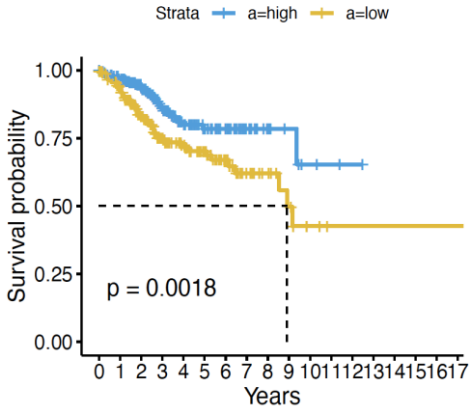

(c)

F3

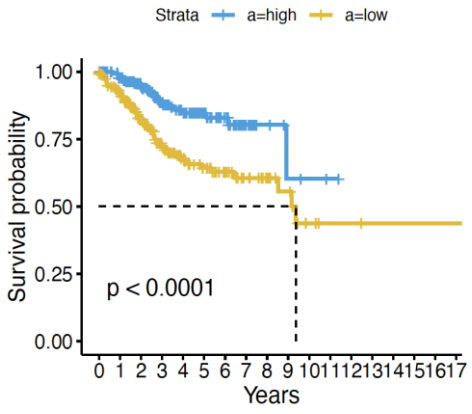

(d)

SCGB2A1

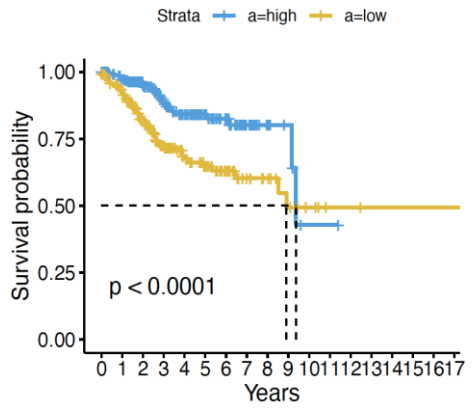

(e)

SERPINA5

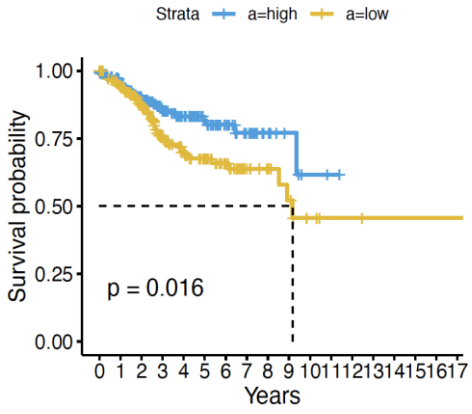

(f)

SLC16A1

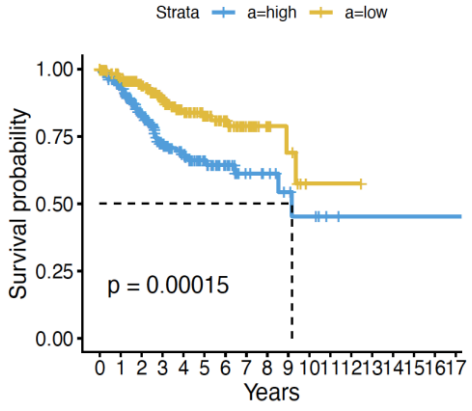

(g)

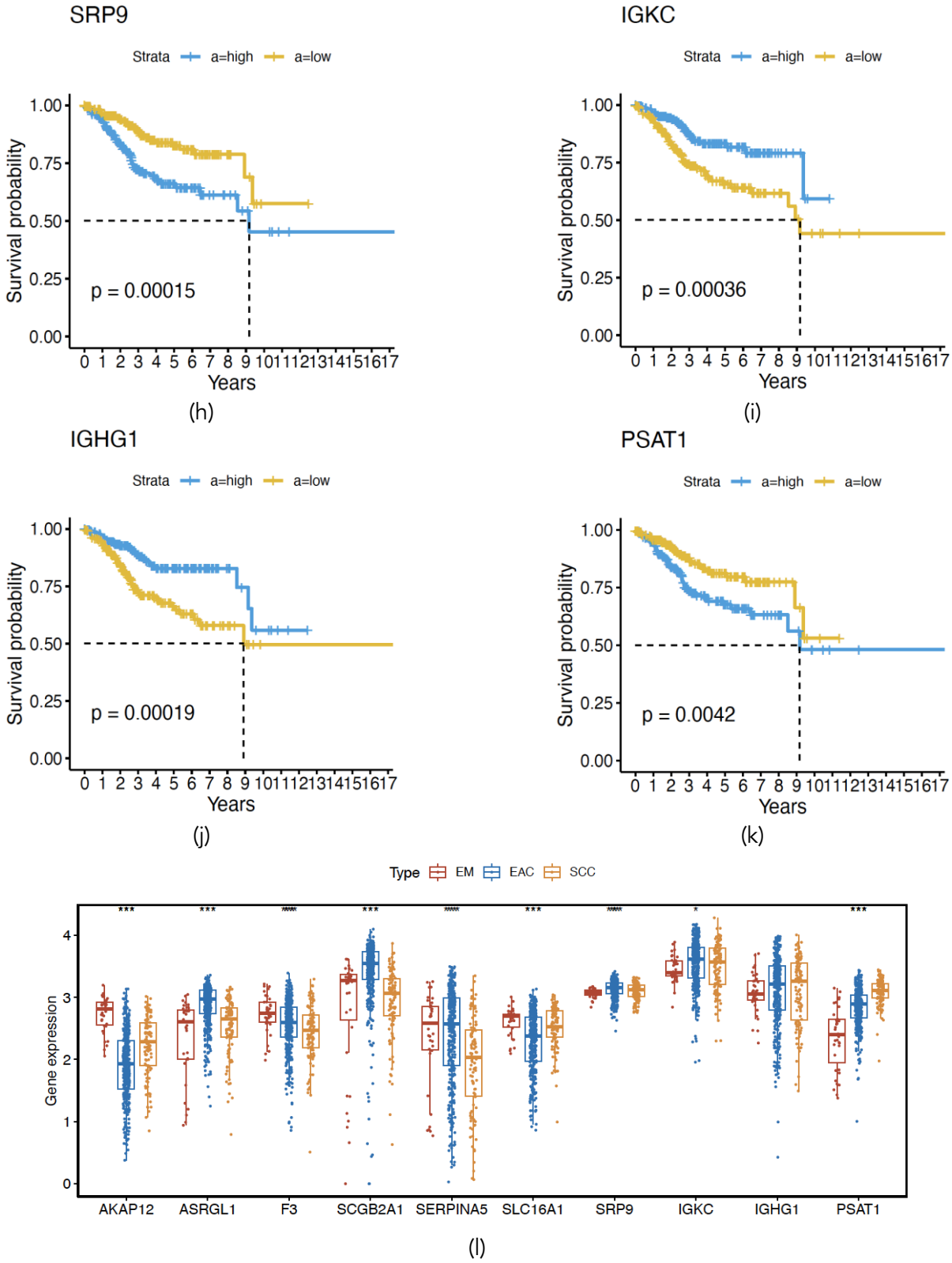

Figure 3. DEGs predicted EC patients survival in the TCGA UCEC dataset: (**a**) Volcano plot showing DEGs between the anti-PD1 non-responder and responder cell type clusters; (**b – k**) The Kaplan-Meir plots for (**b**) AKAP12; (**c**) ASRGL1; (**d**) F3; (**e**) SCGB2A1; (**f**) SERPINA5; (**g**) SLC16A1; (**h**) SRP9; (**i**) IGKC; (**j**) IGHG1; and (**k**) PSAT1 genes in the TCGA dataset, n = 499; (**l**) Boxplot showing expression levels of AKAP12, ASGRL1, F3, SCGB2A1, SERPINA5, SLC16A1, SRP9, IGKC, IGHG1 and PSAT1 genes in the TCGA samples from normal endometrium (EM), n = 35, endometrioid adenocarcinoma (EAC), n = 374, or serous cystadenocarcinoma (SCC), n = 125. The survival analysis was done using the suvminer and survival R packages (version 3.8-3)

CELL-CELL INTERACTION INDICATED EPITHELIAL CELLS AND TREGS MIDKINE-SYNDECAN4 SIGNALING TO ANTI-PD1 THERAPY TOLERANCE

To identify the networks of tumor-promoting and immunosuppressive environments, we analyzed communication between ten cell clusters using CellChat (Figure 4, a; Supplemental Figure 3, a). The number of communications between the cells was calculated (Figure 4, b; Supplemental Figure 3, b). The cell signaling links were identified as the incoming and the outgoing communication patterns of secreting cells (Figure 4, c; Supplemental Figure

3, c, d, e, f). The contribution of ligand-receptor pairs to signaling pathways was calculated (Figure 4, d; Supplemental Figure 3, g). The cell types sending signals were determined as 'sender', and the cell types receiving signals as 'target' (Figure 4, e, f). The Ligand-Receptor (L-R) pairs between the communicating cells were determined (Figure 4, g; Supplemental Figure 3, h, i). The dominant senders (sources) and receivers (targets) in a two-dimensional space were indicated (Figure 4, h, i).

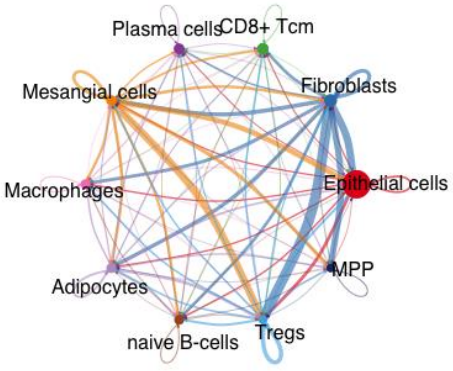

(a)

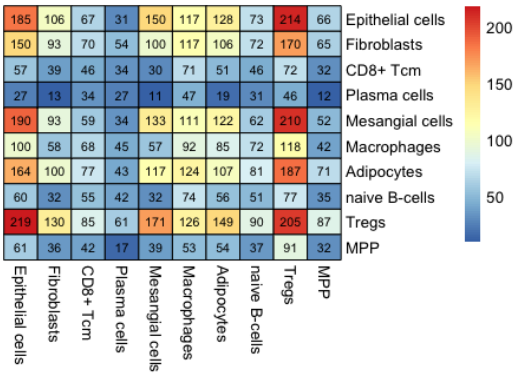

(b)

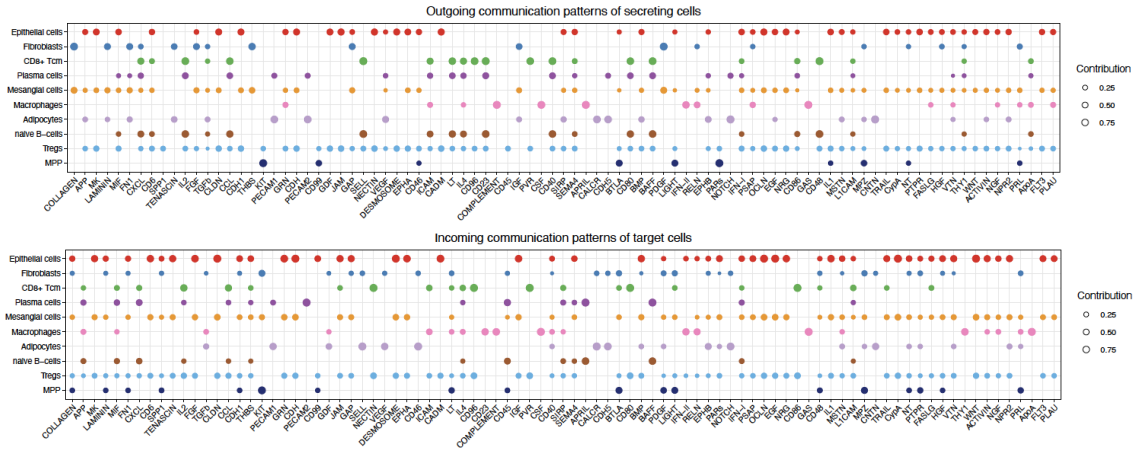

(c)

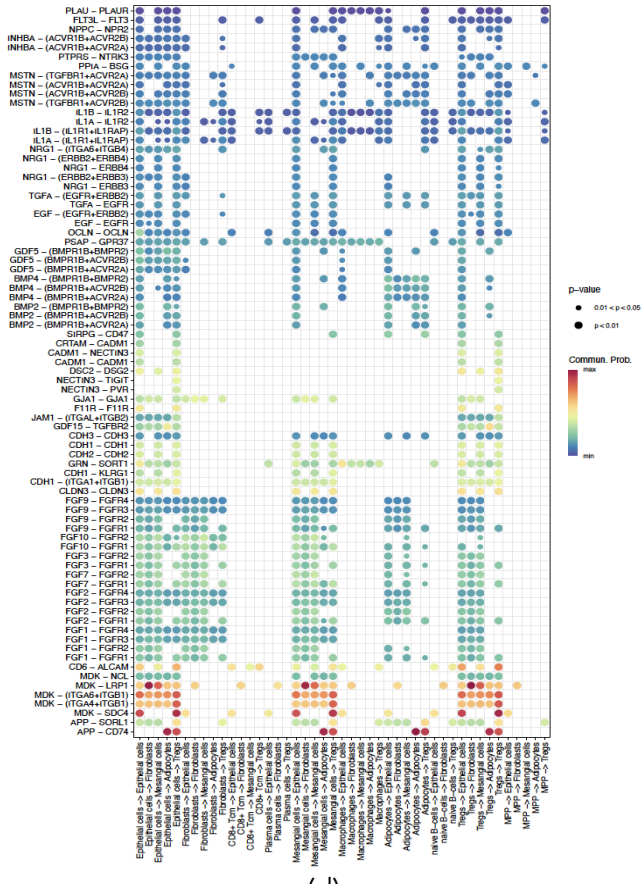

(d)

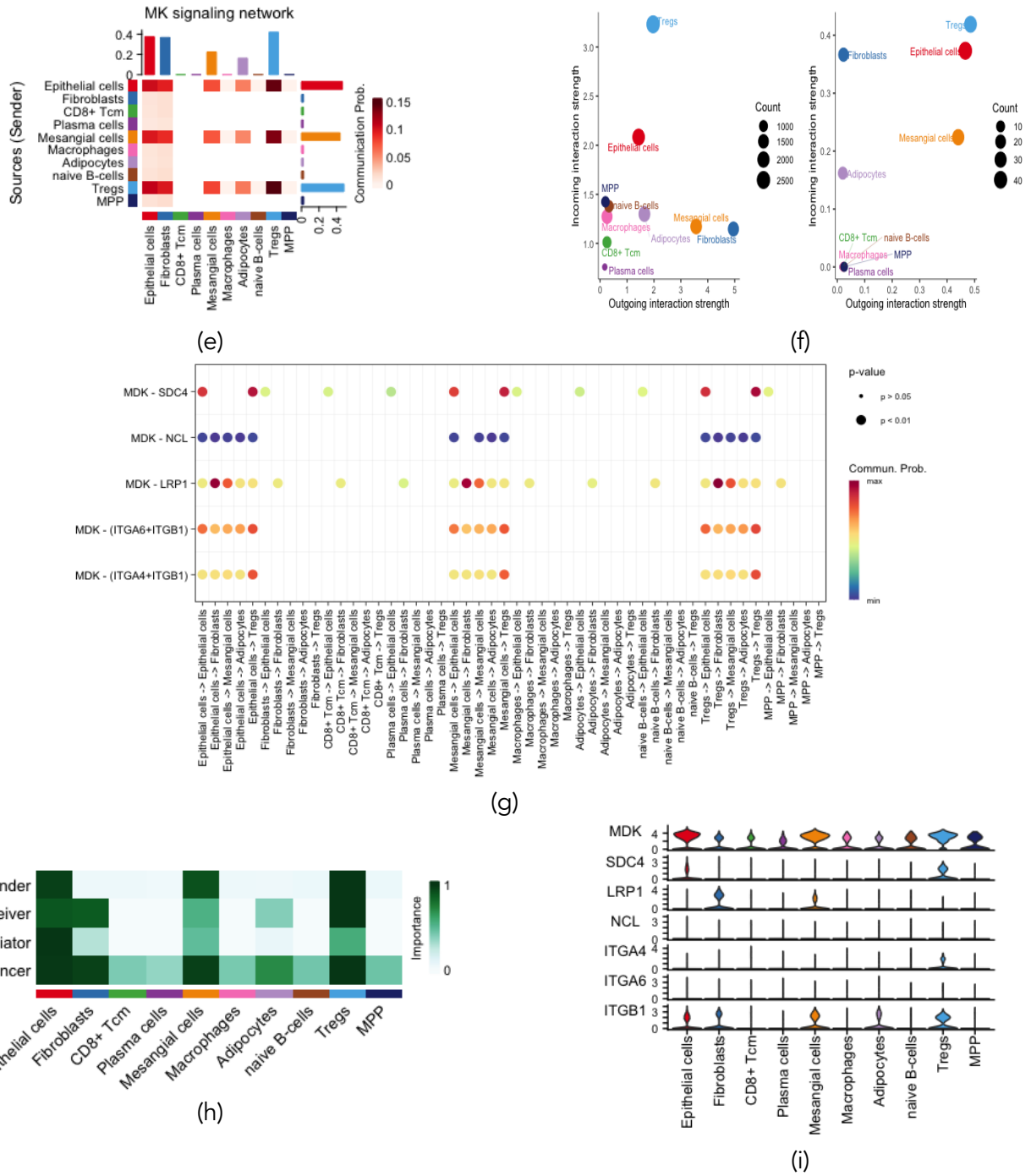

Figure 4. Cell-cell communication indicated epithelial cells and Tregs MK-SDC4 signaling to anti-PD1 therapy tolerance: (**a**) Circle plot showing the interaction strength/weights between the communicating cells. The signal strength is denoted by the line width; (**b**) Heat map showing the number of cell-cell communications between interacting cells; (**c**) The dot plot showing the comparison of outgoing communication patterns of secreting cells (top), and the comparison of incoming communication patterns (bottom); (**d**) The dot plot showing the contribution of ligand-receptor pairs to signaling pathways; (**e**) Heat map showing the inferred intercellular MDK/MK signaling network between interacting cells; (**f**) The graphs showing the signaling effects of all signaling pathways on the aggregated cell-cell communication network (left), and the signaling effects within MK intercellular communication network (right); (**g**) The dot plot showing the comparison of the MDK/MK pathway ligand-receptor pairs contributing to the signaling between cells; (**h**) Heat map showing the importance of interacting cells as the sender, the receiver, the mediator or the influencer of the communication network (network centrality scores); (**i**) The violin plots showing the expression of the seven genes involved in MDK/MK signaling network.

TREGS COLOCALIZED WITH EPITHELIAL CELLS IN THE TUMOR MICROENVIRONMENT

From our single-cell RNA-seq data, the MDK signaling cells included the epithelial cells, fibroblasts, mesangial cells, and Tregs (Figure 4, h). Thus, we predicted the special proximity of the four cell-type marker genes on the endometrial adenocarcinoma ST-seq data. Because the number of tumor epithelial cells increases with EC tumor progression, we assigned the tissue section regions with higher epithelial cells as the tumor. The ST-seq data were generated by sequencing the entire endometrial adenocarcinoma tissue section (Figure 5, a, b). The tissue section

sequenced spots were clustered (Figure 1, c). The epithelial cells, Tregs, mesangial cells, and fibroblast marker-genes expression were spatially identified on the tissue slice (Figure 5, d). To determine colocalization between these cell types, we predicted and mapped the single-cell RNA-seq cell type markers onto the section using spatial pie charts (Figure 5, e).

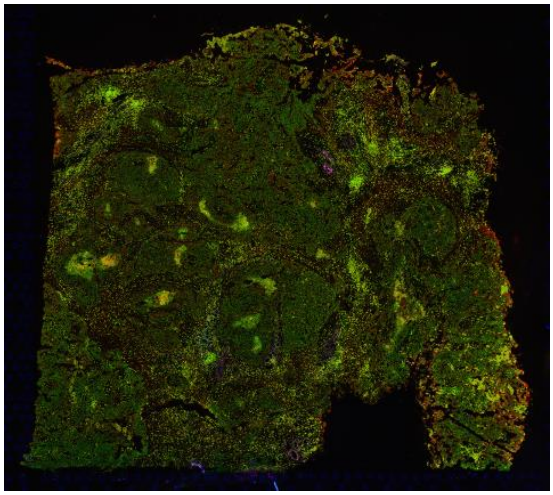

(a)

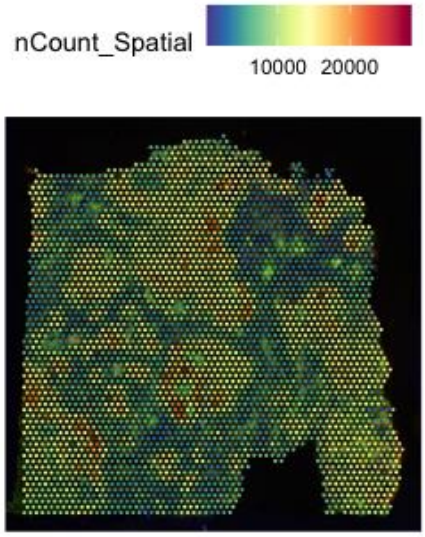

(b)

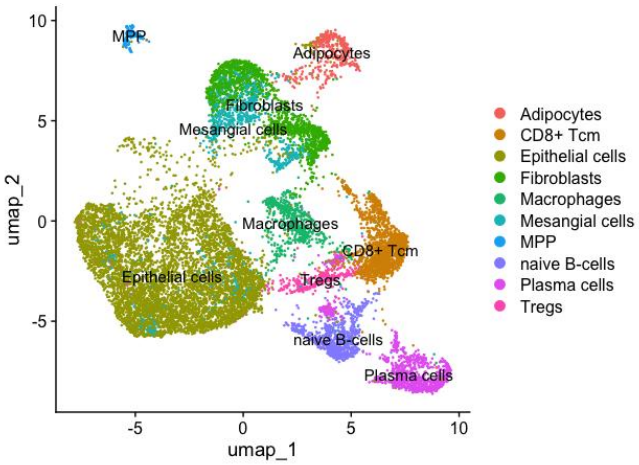

(c)

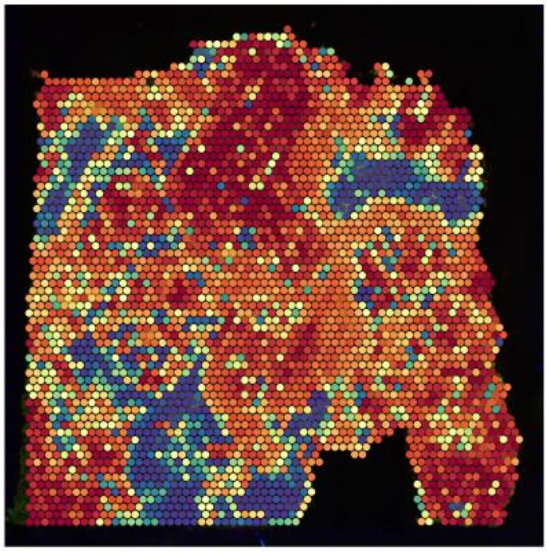

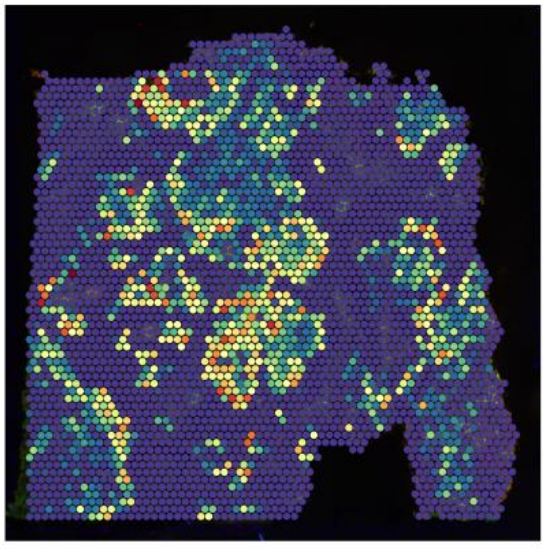

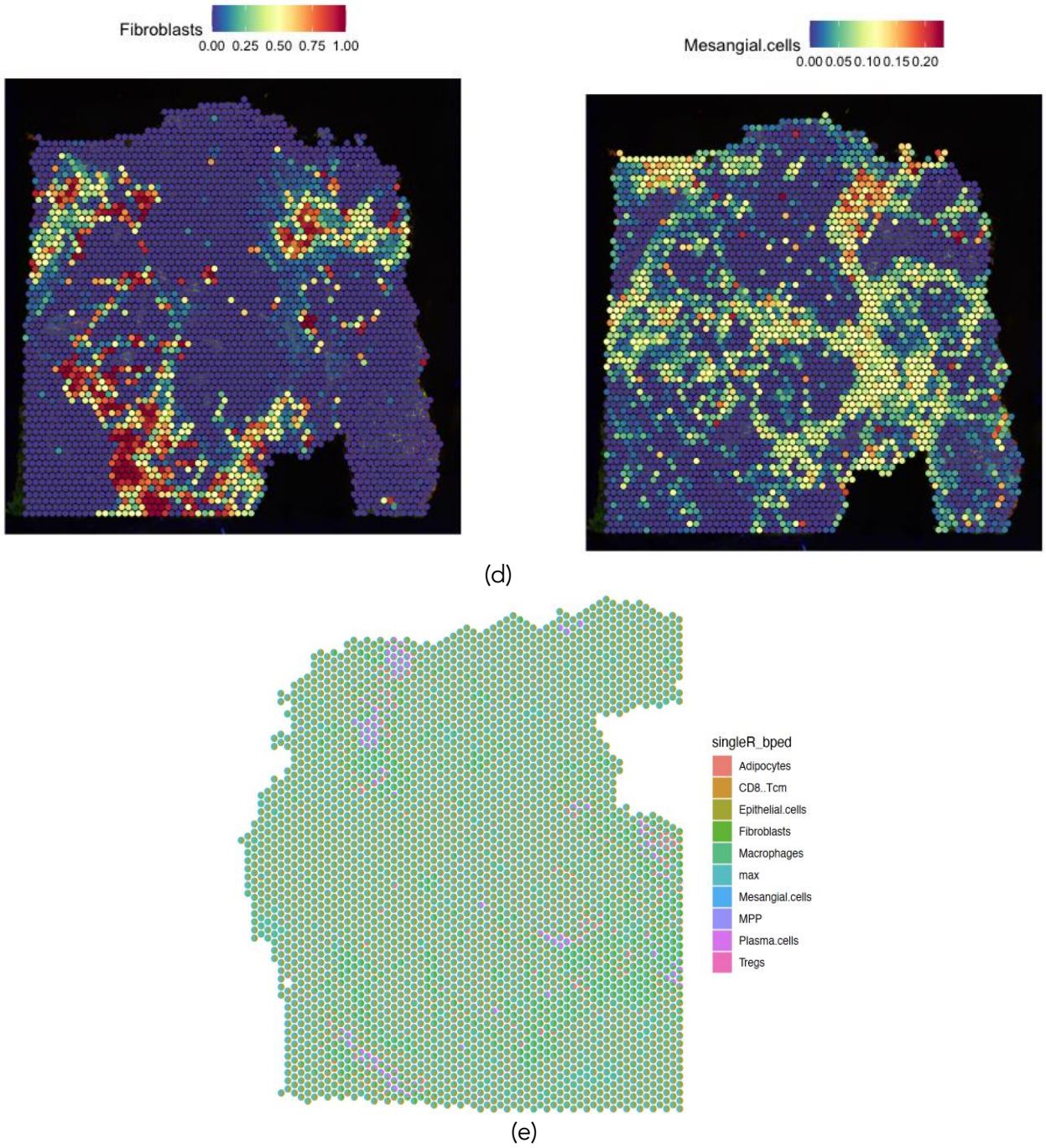

Figure 5. Distribution of colocalized cells between epithelial cells and regulatory T cells (Tregs) in the TME: (**a**) Tumor section stained with DAPI (blue), anti-panCK (Alexa Fluor 488), and anti-CD45 (Alexa Fluor 647) used to generate the ST-seq data; (**b**) Slice showing spatial sequencing reads for each spot; (**c**) UMAP showing single-cell RNA-seq data cell clusters; (**d**) Predicted abundance within each capture spot for the cell types; (**e**) Spatial scatter pie plot showing the cell proportions from the reference atlas within capture spots in the endometrial adenocarcinoma tissue section. 'max' in the key represents Naïve B cells.

ELEVATED EXPRESSION LEVELS OF MIDKINE AND SYNDECAN4 PREDICT POOR PROGNOSIS IN ENDOMETRIAL CANCER PATIENTS

High MDK expression is associated with high tumor-associated macrophages (TAMs), regulatory T cells (Tregs), and poor cancer prognosis[7,56,57]. MDK has shown potential in the prognosis and diagnosis of ovarian[58], gallbladder[59], and colorectal[60] cancers. We did the survival analysis of the TCGA UCEC dataset using MDK pathway genes (midkine (MDK), syndecan-4 (SDC4), low-density lipoprotein receptor-related proteins 1 (LRP1), nucleolin (NCL), integrin subunit alpha 4 (ITGA4), integrin subunit alpha 6 (ITGA6), and integrin subunit beta 1 (ITGB1) (Figure 6, a; Supplemental Figure 4, a, b, c, d, e, f). Finally, we analyzed the expression of MDK pathway genes (MDK, SDC4, LRP1, NCL, ITGA4, ITGA6, ITGB1) in the TCGA UCEC data set using the estimate score in R software (Figure 6, b).

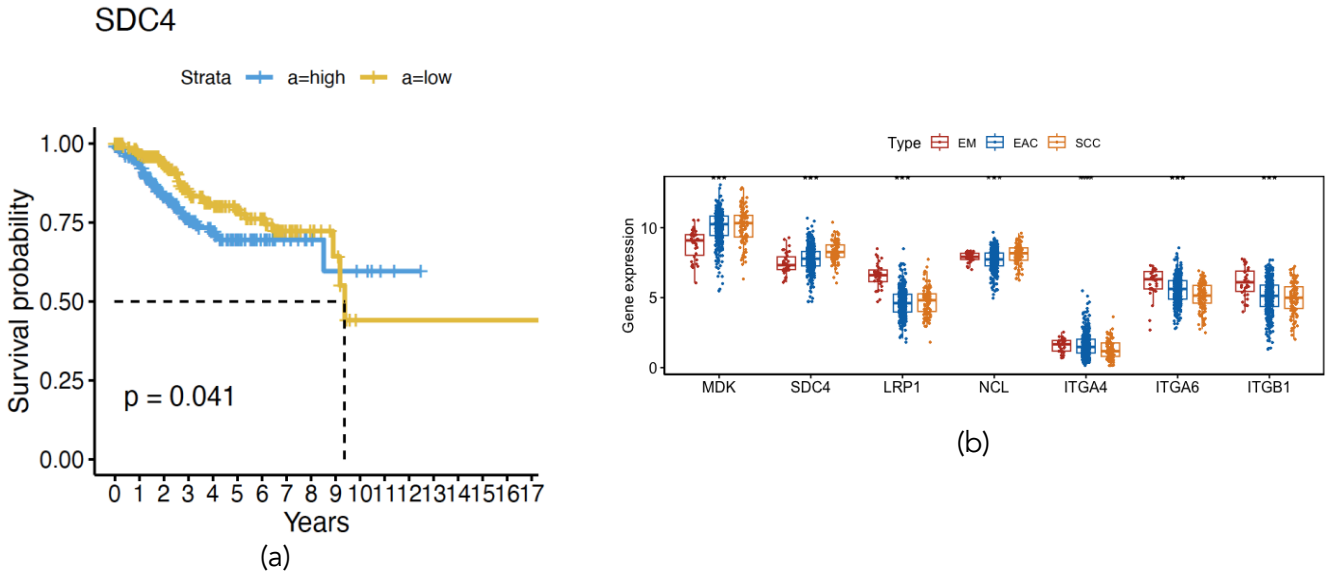

Figure 6. Clinical significance of MDK and SDC4 expression in EC patients: (**a**) The Kaplan-Meir plots for SCD4 gene in the TCGA dataset, n = 499; (**b**) Boxplot showing expression levels of MDK, SCD4, LRP1, NCL, ITGA4, ITGA6, and ITGB1 genes in the TCGA samples from normal endometrium (EM), n = 35, endometrioid adenocarcinoma (EAC), n = 374, or serous cystadenocarcinoma (SCC), n = 125. The survival analysis was done using the suvminer and survival R packages (version 3.8-3)

Discussion

We analyzed publicly available single-cell RNA-seq data for anti-PD1 therapy responder and non-responder EC samples. The study revealed the transcriptional and regulatory landscape of anti-PD1 therapy responder and non-responder of EC tumors at single-cell resolution. This approach enabled the understanding of the TME by examining cell-cell communications.

In this study, samples from two EC patients treated with anti-PD1 Pembrolizumab 200 mg intravenously in combination with a pan-kinase inhibitor Lenvatinib 20 mg orally. There was a progressive disease in the Case B patient, and we treated it as an anti-PD1 non-responder. There was a partial response in the Case A patient, and we treated it as an anti-PD1 responder. The RNA sequencing platform was of high quality because we identified WAP Four-Disulfide Core Domain 2 (WFDC2) gene as the highest expressed gene in the cells (Figure 1, a). The WFDC2 gene is used as a diagnostic marker for endometrial adenocarcinoma. In addition, the gene counts for the samples were not significantly different (Supplemental Figure 1, a). After quality filtering, 18,082 genes were detected in 17,593 cells. Cells were clustered into 19 clusters and annotated into ten cell types based on the marker gene expression in the Blueprint Encode Data (BPED) cell library. The distinctly annotated cells were adipocytes, CD8+ T cell memory, epithelial cells, fibroblasts, macrophages, mesangial cells, multipotent progenitor (MPP) cells, naïve B-cells, plasma cells, and Tregs. The cells represented both immune and non-immune cell types. The cells had minimal differences when compared to the original study[17]. This is expected when analyzing high-dimensional data like single-cell RNA -seq data. We used the BPED library accessed by singleR package, but Chen et al.[17] used a different marker gene library. The epithelial cells were the most abundant in both studies.

The GO and KEGG pathway analysis identified the methylation pathway (adjusted p <0.029) in epithelial cells as the pathway upregulated in anti-PD1 responder compared to non-responder. Hypomethylation is one of the initial events that lead to EC carcinogenesis. Immune response activating cell surface receptor signaling pathway (adjusted p <0.009) was enriched in adipocytes. This supports the implication of obesity as a risk factor in EC. The CD8+ T central memory (CD8+ Tcm) cells mitochondrion organization pathway (adjusted p <0.034) was enriched that determine the memory T cell fate[61] (Figure 2, a). Other pathways were regulation of GTPase activity, mitochondrial organization, and immune response signaling. The GSVA and pseudo bulk DE gene analysis validated these results. The GSVA results showed uniform clustering among different cell types from different samples (Figure 2, b). Most of the pathways enriched in single-cell RNA-seq analysis were also enriched in the pseudo bulk pathway analysis. They included the T cell receptor signaling pathway (adjusted p <0.009) (Figure 2, c,

d, e). The top DE gene sets from the epithelial cell lineage successfully predicted the anti-PD1 therapy outcome using various ML methods (area under the curve (AUC > 0.99) (Table 1). The neural network (NN) method achieved the highest prediction scores for cell types in the BPED and IMMU libraries, whereas the LASSO method achieved the best scores for cell types in the HPCA and NHD libraries (Table 1). In this study, we used the BPED library cell annotation because it had both tumor cells and immune cells. The top ten DE genes modulate tumor immunity in cancer and shape the outcome of immunotherapies like anti-PD1 (Table 2).

We tested the utility of the top single-cell RNA-seq DE gene sets from the epithelial cell lineage on patient survival. As expected, the expression of the DE genes, 12 of the 20 genes, correlated with prognosis in the TCGA UCEC patient data (Figure 3, b - k). High gene expression of AKAP12, SLC16A1, SRP9, PSAT1, and NUCKS1 correlated with poor EC patients survival (Figure 3, a, g, h, k), whereas high gene expression of ASRGL1, F3, SCGB2A1, SERPINA5, IGKC, IGHG1, and WFDC2 (Figure 3, c, d, e, f, i, j), correlated with better EC patient survival. The best therapeutic target gene is one that is upregulated in tumors and is associated with poor prognosis. We compared the expression of genes associated with poor EC patient survival in the TCGA UCEC dataset. SRP9 and PSAT1 were upregulated in tumors and associated with poor prognosis (Figure 3, h, k, l). These data suggest that SRP9 and PSAT1 may be targets in the EC therapy.

Regulation of the interaction between cancer cells and immune cells plays a crucial role in immune suppression in malignancy[62]. Our cell-cell communication analysis revealed that the highest communications were between epithelial cells and Tregs, with 219 communications. Other cell types with high traffic interactions were mesangial cells, adipocytes, and fibroblasts, respectively (Figure 4, b). The cells interacted via 89 signaling links. The Collagen, amyloid precursor protein (APP), and MDK/MK pathways were the top three strongest links. Epithelial cells, mesangial cells, and Tregs emitted and received the strongest signals compared to other cells (Figure 4, c). We discovered that the three cell types, together with fibroblasts, interacted through MDK pathway receptor-ligand pairs (Figure 4, d). Epithelial cells, mesangial cells, and Tregs were the signal sources, while Tregs were the major receivers of the MDK signal (Figure 4, e). This finding is corroborated by the shift to the right of epithelial cells, mesangial cells, and Tregs in the MDK pathway signaling effect, compared to the aggregate signaling pathways effect (Figure 4, f, right). We found epithelial cells and Tregs cells were contacted through Ligand-Receptor (L-R) pairs of MDK -SDC4 in the MK signal pathway (Figure 4, g). These data were supported by the MDK network centrality score, indicating Tregs as the major signal receiver (Figure 4, h). MDK was mainly expressed in epithelial cells, mesangial cells, and Tregs, and SDC4 was expressed mainly in Tregs (Figure 4, i). Tregs are believed to cause immunosuppression in the TME of various cancers, including EC[63]. In this study, we identified that Tregs contribute to immune suppression in an anti-PD1-tolerant tumor. In the EC TME, cell communication is mediated mainly by MDK. MDK is a secreted heparin-binding growth factor that drives immune cell chemotaxis[64]. Elevated MDK in epithelial cells has been shown to induce TAM and T cell-mediated immune tolerance in melanoma, colorectal, and gallbladder cancer[56,57,59]. Herein, MDK was upregulated in epithelial cells, mesangial cells, and Tregs. The TCGA UCEC data indicated that MDK was elevated in tumors compared to normal adjacent tissues (NATs). Therefore, MDK may serve as an important target in immunotherapy.

However, MDK is involved in normal cell growth, cell division, and the regulation of blood vasculature development and function[65]. Thus, to reduce the MDK off-target effects, it's logical to target other molecules within the MDK signaling pathway. We identified the SDC4 receptor on the Tregs as the receiver of the MDK signal in anti-PD1 therapy non-responder. From our single-cell RNA-seq data, the MDK signaling cells included the epithelial cells, fibroblasts, mesangial cells, and Tregs (Figure 4, h). Thus, we predicted the special proximity of the four cell-type marker genes on the endometrial adenocarcinoma ST-seq data. The epithelial cells, Tregs, mesangial cells, and fibroblast marker-genes expression were spatially identified on the tissue slice (Figure 5, c). Because the number of tumor epithelial cells increases with EC tumor progression, we assigned the tissue section regions with higher epithelial cells as the

tumor. Tregs colocalized with epithelial cells in the tumor regions (Figure 5, d (top), e). However, the mesangial cells and fibroblasts are localized mainly in the stromal regions (Figure 5, d (bottom and bottom right). This data suggests that epithelial cells expressing high levels of MDK are in proximity to Tregs, allowing for optimal crosstalk. SDC4 is also associated with the development of breast, prostate, osteosarcoma, pancreas, and colorectal cancers[66–69]. It is an endogenous membrane-associated receptor that regulates cell adhesion and migration in cancer initiation and progression. SDC4 regulates signaling pathways that involve protein kinase C-alpha, Rac 1 GTPase activity, intracellular calcium, and focal adhesion kinase[70–74]. Yu et al.[57] predicted that NCL mediates MDK signaling in EC to induce immune suppression. NCL is a protein found on the cell membrane, in the nucleoplasm, and the cytoplasm of cells[75], and is involved in angiogenesis, apoptosis, and cell proliferation[76]. Herein, NCL signaling interaction was the least among the MDK ligand-receptor pairs. This indicates SDC4 as the major MDK-receptor for immune tolerance to anti-PD1 therapy.

High MDK expression is associated with high tumor-associated macrophages (TAMs), regulatory T cells (Tregs), and poor cancer prognosis[7,56,57]. MDK has shown potential in the prognosis and diagnosis of ovarian[58], gallbladder[59], and colorectal[60] cancers. We performed a survival analysis of the TCGA UCEC dataset using MDK receptors identified in this study. However, only high expression of the SDC4 gene had a significant effect on the survival outcome (Figure 6, a). Finally, the SDC4 gene was overexpressed in the TCGA UCEC dataset (Figure 6, b).

There are limitations to the present study, including a lack of substantial reference data for EC. The data used was the only single-cell RNA-seq data comparing ati-PD1 responders and non-responders. Second, we did not validate the importance of the MDK-SDC4 signaling in EC with in vivo or in vitro experiments. Third, the TCGA UCEC dataset used in the study lacked anti-PD1 intervention. Further studies are needed to validate our results in a larger sample size and confirm the importance of the MDK-SDC4 signaling in both in vitro and in vivo experiments.

In summary, the single-cell RNA-seq analysis performed herein revealed MDK-SDC4 signaling as the driver inducing the immune suppression phenotype in the anti-PD1 therapy non-responder. These findings suggest that blocking the MDK-SDC4 signal might help to overcome the anti-PD1 therapy tolerance in EC. These results show novel potential immunotherapeutic targets in EC.

Conclusion

In this study, we integrated single-cell RNA sequencing, spatial transcriptomics, and clinical transcriptomic datasets to investigate mechanisms underlying heterogeneity in anti-PD1 therapy response in endometrial cancer (EC). This multimodal approach enabled high-resolution characterization of the tumor microenvironment and identified immunoregulatory cell-cell communication networks distinguishing responders from non-responders. Epithelial cells emerged as a central signaling hub, with epithelial-derived midkine (MDK) engaging syndecan-4 (SDC4) on regulatory T cells to promote an immunosuppressive microenvironment. Spatial analyses confirmed co-localization of Tregs and epithelial cells within tumor regions, while machine learning models demonstrated the predictive value of epithelial transcriptional programs for treatment tolerance. Elevated SDC4 expression was also associated with adverse outcomes in TCGA UCEC data, supporting clinical relevance.

These findings identify MDK-SDC4 signaling as a key mechanism of immune evasion in EC that may limit immune checkpoint blockade efficacy. Unlike prior models emphasizing nucleolin as the primary MDK receptor, our results implicate SDC4 as the dominant mediator in anti-PD1-resistant EC, highlighting tumor-specific receptor usage and positioning SDC4 as a potential therapeutic target downstream of MDK.

More broadly, this work demonstrates the value of single-cell approaches for dissecting immunotherapy resistance in heterogeneous cancers. However, the study is limited by sample size, lack of functional validation, and non-uniform checkpoint therapy exposure in TCGA survival analyses. Future experimental and prospective clinical studies are needed to establish causality and determine whether targeting the MDK-SDC4 axis restores checkpoint sensitivity.

Overall, our integrative analysis identifies MDK-SDC4 signaling as a central driver of immune

suppression and anti-PD1 tolerance in EC, providing a testable therapeutic strategy to enhance immunotherapy response in patients with advanced or recurrent disease.

Graphical Abstract

MDK-SDC4 Signaling in Endometrial Cancer

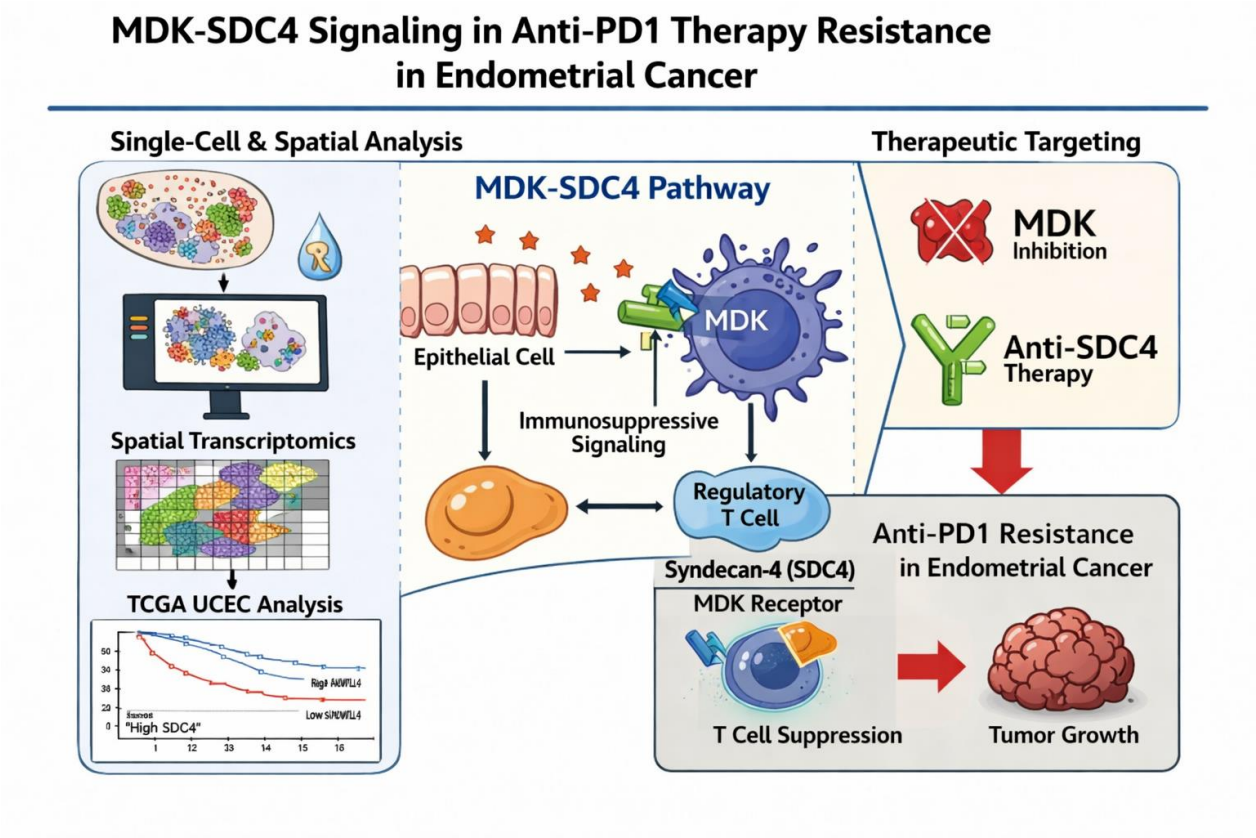

Conflict of Interest Statement:

The authors declare no conflicts of interest.

Funding Statement:

The National Institute of Health/The National Cancer Institute (P30CA168524).

Acknowledgements:

Not Applicable.

Institutional Review Board Statement:

Not applicable.

Informed Consent Statement:

Not applicable.

Data Availability Statement:

The study used publicly available datasets, the accession numbers of which are included in the article. The ST-seq data were accessed on the 10X Genomics website (https://www.10xgenomics.com/datasets).
The codes used in this work were modifications of publicly available code from the Rahul Satija, Satija Lab, and Collaborators website (https://satijalab.org/seurat/).

References:

1. Lu KH, Broaddus RR. Endometrial Cancer. Longo DL, ed. *N Engl J Med*. 2020;383(21):2053-2064. doi:10.1056/NEJMra1514010

2. Endometrial Cancer Treatment (PDQ®) - NCI. June 9, 2023. Accessed June 20, 2023. https://www.cancer.gov/types/uterine/hp/endometrial-treatment-pdq

3. Lortet-Tieulent J, Ferlay J, Bray F, Jemal A. International patterns and trends in endometrial cancer incidence, 1978–2013. *JNCI: Journal of the National Cancer Institute*. 2018;110(4):354-361.

4. Gatius S, Cuevas D, Fernández C, et al. Tumor heterogeneity in endometrial carcinoma: practical consequences. *Pathobiology*. 2018;85(1-2):35-40.

5. Guo Y e, Li Y, Cai B, et al. Phenotyping of immune and endometrial epithelial cells in endometrial carcinomas revealed by single-cell RNA sequencing. *Aging (Albany NY)*. 2021;13(5):6565.

6. Sikkandhar MG, Nedumaran AM, Ravichandar R, et al. Theranostic probes for targeting tumor microenvironment: an overview. *International journal of molecular sciences*. 2017;18(5):1036.

7. Hashimoto M, Kojima Y, Sakamoto T, et al. Spatial and single-cell colocalisation analysis reveals MDK-mediated immunosuppressive environment with regulatory T cells in colorectal carcinogenesis. *EBioMedicine*. 2024;103. Accessed July 31, 2025. https://www.thelancet.com/journals/ebiom/article/PIIS2352-3964(24)00137-3/fulltext

8. Chen L, Han X. Anti–PD-1/PD-L1 therapy of human cancer: past, present, and future. *The Journal of clinical investigation*. 2015;125(9):3384-3391.

9. Jiang X, Wang J, Deng X, et al. Role of the tumor microenvironment in PD-L1/PD-1-mediated tumor immune escape. *Mol Cancer*. 2019;18(1):10. doi:10.1186/s12943-018-0928-4

10. Le DT, Uram JN, Wang H, et al. PD-1 Blockade in Tumors with Mismatch-Repair Deficiency. *N Engl J Med*. 2015;372(26):2509-2520. doi:10.1056/NEJMoa1500596

11. Zhao J, Jaffe A, Li H, et al. Detection of differentially abundant cell subpopulations in scRNA-seq data. *Proc Natl Acad Sci USA*. 2021;118(22):e2100293118. doi:10.1073/pnas.2100293118

12. Krieg C, Nowicka M, Guglietta S, et al. High-dimensional single-cell analysis predicts response to anti-PD-1 immunotherapy. *Nature medicine*. 2018;24(2):144-153.

13. Miller BC, Sen DR, Al Abosy R, et al. Subsets of exhausted CD8+ T cells differentially mediate tumor control and respond to checkpoint blockade. *Nature immunology*. 2019;20(3):326-336.

14. Sade-Feldman M, Yizhak K, Bjorgaard SL, et al. Defining T cell states associated with response to checkpoint immunotherapy in melanoma. *Cell*. 2018;175(4):998-1013.

15. Human Ovarian Cancer: Whole Transcriptome Analysis. Stains: DAPI, Anti-PanCK, Anti-CD45. 10x Genomics. Accessed August 6, 2025. https://www.10xgenomics.com/datasets/human-ovarian-cancer-whole-transcriptome-analysis-stains-dapi-anti-pan-ck-anti-cd-45-1-standard-1-2-0

16. Jin S, Guerrero-Juarez CF, Zhang L, et al. Inference and analysis of cell-cell communication using CellChat. *Nature communications*. 2021;12(1):1088.

17. Chen J, Song Y, Huang J, Wan X, Li Y. Integrated single-cell RNA sequencing and spatial transcriptomics analysis reveals the tumour microenvironment in patients with endometrial cancer responding to anti-PD-1 treatment. *Clinical and Translational Medicine*. 2024;14(4):e1668.

18. Hao Y, Hao S, Andersen-Nissen E, et al. Integrated analysis of multimodal single-cell data. *Cell*. 2021;184(13):3573-3587.

19. Ekiz HA, Conley CJ, Stephens WZ, O'Connell RM. CIPR: a web-based R/shiny app and R package to annotate cell clusters in single cell RNA sequencing experiments. *BMC Bioinformatics*. 2020;21(1):191. doi:10.1186/s12859-020-3538-2

20. Fernández JM, de la Torre V, Richardson D, et al. The BLUEPRINT data analysis portal. *Cell systems*. 2016;3(5):491-495.

21. Feingold EA, Good PJ, Guyer MS, et al. The ENCODE (ENCyclopedia of DNA elements) project. *Science*. 2004;306(5696):636-640.

22. Muthukrishnan R, Rohini R. LASSO: A feature selection technique in predictive modeling for machine learning. In: *2016 IEEE International Conference on Advances in Computer Applications (ICACA)*. Ieee; 2016:18-20. Accessed July 27, 2025. https://ieeexplore.ieee.org/abstract/document/7887916/

23. Rajan MP. An Efficient Ridge Regression Algorithm with Parameter Estimation for Data Analysis in Machine Learning. *SN COMPUT SCI*. 2022;3(2):171. doi:10.1007/s42979-022-01051-x

24. Zou H, Hastie T. Regularization and variable selection via the elastic net. *Journal of the Royal Statistical Society Series B: Statistical Methodology*. 2005;67(2):301-320.

25. Chen T, Guestrin C. XGBoost: A Scalable Tree Boosting System. In: *Proceedings of the 22nd ACM SIGKDD International Conference on Knowledge Discovery and Data Mining*. ACM; 2016:785-794. doi:10.1145/2939672.2939785

26. Zhao S, Zhang B, Yang J, Zhou J, Xu Y. Linear discriminant analysis. *Nature Reviews Methods Primers*. 2024;4(1):70.

27. Brickley MR, Shepherd JP, Armstrong RA. Neural networks: a new technique for development of decision support systems in dentistry. *Journal of dentistry*. 1998;26(4):305-309.

28. Breiman L. Random Forests. *Machine Learning*. 2001;45(1):5-32. doi:10.1023/A:1010933404324

29. Rokach L, Maimon O. Classification Trees. In: Maimon O, Rokach L, eds. *Data Mining and Knowledge Discovery Handbook*. Springer US; 2009:149-174. doi:10.1007/978-0-387-09823-4_9

30. Liberzon A, Subramanian A, Pinchback R, Thorvaldsdóttir H, Tamayo P, Mesirov JP. Molecular signatures database (MSigDB) 3.0. *Bioinformatics*. 2011;27(12):1739-1740.

31. Love MI, Huber W, Anders S. Moderated estimation of fold change and dispersion for RNA-seq data with DESeq2. *Genome Biol*. 2014;15 (12):550. doi:10.1186/s13059-014-0550-8

32. Hänzelmann S, Castelo R, Guinney J. GSVA-The Gene Set Variation Analysis Package. Published online 2011. Accessed July 27, 2025. https://bioconductor.statistik.tu-dortmund.de/packages/2.9/bioc/vignettes/GSVA/inst/doc/GSVA.pdf

33. Gy\Horffy B. Integrated analysis of public datasets for the discovery and validation of survival-associated genes in solid tumors. *The Innovation*. 2024;5(3). Accessed July 30, 2025. https://www.cell.com/the-innovation/fulltext/S2666-6758(24)00063-8

34. Chuluyan E, Ambrosi N, Fraunhoffer N, et al. Secretory leukocyte proteinase inhibitor: A key player in the dialogue between the tumor and its microenvironment in pancreatic cancer patients. *JCO*. 2022;40(4_suppl):592-592. doi:10.1200/JCO.2022.40.4_suppl.592

35. Sun L, Ke M, Wang X, et al. FAP^{high} α-SMA^{low} cancer-associated fibroblast-derived SLPI protein encapsulated in extracellular vesicles promotes ovarian cancer development via activation of PI3K/AKT and downstream signaling pathways. *Molecular Carcinogenesis*. 2022;61(10):910-923. doi:10.1002/mc.23445

36. Huang L, Li W, Lu Y, Ju Q, Ouyang M. Iron metabolism in colorectal cancer. *Frontiers in Oncology*. 2023;13:1098501.

37. Mhawech-Fauceglia P, Wang D, Samrao D, Liu S, Pejovic T. Trefoil factor family 3 (TFF3) expression and its interaction with estrogen receptor (ER) in endometrial adenocarcinoma. *Gynecologic oncology*. 2013;130(1):174-180.

38. Lacroix M. Significance, detection and markers of disseminated breast cancer cells. *Endocrine-related cancer*. 2006;13(4):1033-1067.

39. Huang F, Wang Y, Shao Y, et al. M2 Macrophage Classification of Colorectal Cancer Reveals Intrinsic Connections with Metabolism Reprogramming and Clinical Characteristics. *PGPM*. 2024;Volume 17:383-399. doi:10.2147/PGPM.S458798

40. Li L, Chao Z, Waikeong U, et al. Metabolic classifications of renal cell carcinoma reveal intrinsic connections with clinical and immune characteristics. *J Transl Med*. 2023;21(1):146. doi:10.1186/s12967-023-03978-y

41. Ferreri AJ, Calimeri T, Conte GM, et al. R-CHOP preceded by blood-brain barrier permeabilization with engineered tumor necrosis factor-α in primary CNS lymphoma. *Blood, The Journal of the American Society of Hematology*. 2019;134(3):252-262.

42. Ji R, Wang Y, Pan D, et al. NUCB2 inhibition antagonizes osteosarcoma progression and promotes anti-tumor immunity through inactivating NUCKS1 /CXCL8 axis. *Cancer letters*. 2024;591:216893.

43. Soliman NA, Zineldeen DH, El-Khadrawy OH. Effect of NUCKS-1 overexpression on cytokine profiling in obese women with breast cancer. *Asian Pacific Journal of Cancer Prevention*. 2014;15 (2):837-845.

44. Luo Z, Chen X, Zhang Y, et al. Development of a metastasis-related immune prognostic model of metastatic colorectal cancer and its usefulness to immunotherapy. *Frontiers in cell and developmental biology*. 2021;8:577125.

45. Wang S, Zhang W, Wu X, et al. Comprehensive analysis of T-cell regulatory factors and tumor immune microenvironment in stomach adenocarcinoma. *BMC Cancer*. 2024;24(1):570. doi:10.1186/s12885-024-12302-w

46. Yu Q, Xie T, Zhang Y, et al. Exploration of SERPINA family functions and prognostic value in breast cancer based on transcriptome and in vitro analysis. *Environmental Toxicology*. 2024;39(4):1951-1967. doi:10.1002/tox.24079

47. Ortiz-Barahona V, Soler M, Davalos V, et al. Epigenetic inactivation of the 5-methylcytosine RNA methyltransferase NSUN7 is associated with clinical outcome and therapeutic vulnerability in liver cancer. *Mol Cancer*. 2023;22(1):83. doi:10.1186/s12943-023-01785-z

48. Thaventhiran JE, Lango Allen H, Burren OS, et al. Whole-genome sequencing of a sporadic primary immunodeficiency cohort. *Nature*. 2020;583(7814):90-95.

49. Chen L, Li Y, Deng X. Comprehensive analysis of pan-cancer reveals the potential of SLC16A1 as a prognostic and immunological biomarker. *Medicine*. 2023;102(11):e33242.

50. Nabet BY, Qiu YU, Shabason JE, et al. Exosome RNA unshielding couples stromal activation to pattern recognition receptor signaling in cancer. *Cell*. 2017;170(2):352-366.

51. Jandova J, Wondrak GT. Genomic GLO1 deletion modulates TXNIP expression, glucose metabolism, and redox homeostasis while accelerating human A375 malignant melanoma tumor growth. *Redox Biology*. 2021;39:101838.

52. Liu K, Hoover AR, Sun Y, et al. Anti-tumor effects on tumor-infiltrating natural killer cells by localized ablative immunotherapy and immune checkpoint inhibitors: An integrated and comparative study using scRNAseq analysis. *Cancer Letters*. Published online 2025:217825.

53. Wang C, Lu M, Chen C, et al. Integrating scRNA-seq and Visium HD for the analysis of the tumor microenvironment in the progression of colorectal cancer. *International Immunopharmacology*. 2025;145:113752.

54. Zhou L, Yu G, Zheng Z, Xu B. IGHA1 and IGHG1 Expression Panel Predicts Anti-PD-L1 Response in Muscle-Invasive Bladder Cancer. *Molecular Carcinogenesis*. 2025;64(11):1942-1955. doi:10.1002/mc.70033

55. Zheng P, Hu Z, Shen Y, et al. PSAT1 impairs ferroptosis and reduces immunotherapy efficacy via GPX4 hydroxylation. *Nature Chemical Biology*. Published online 2025:1-13.

56. Cerezo-Wallis D, Contreras-Alcalde M, Troulé K, et al. Midkine rewires the melanoma microenvironment toward a tolerogenic and immune-resistant state. *Nature medicine*. 2020;26(12):1865-1877.

57. Yu X, Xie L, Ge J, Li H, Zhong S, Liu X. Integrating single-cell RNA-seq and spatial transcriptomics reveals MDK-NCL dependent immunosuppressive environment in endometrial carcinoma. *Frontiers in Immunology*. 2023;14:1145300.

58. Curiel TJ, Coukos G, Zou L, et al. Specific recruitment of regulatory T cells in ovarian carcinoma fosters immune privilege and predicts reduced survival. *Nature medicine*. 2004;10(9):942-949.

59. Zhang Y, Zuo C, Liu L, et al. Single-cell RNA-sequencing atlas reveals an MDK-dependent immunosuppressive environment in ErbB pathway-mutated gallbladder cancer. *Journal of hepatology*. 2021;75(5):1128-1141.

60. Ye C, Qi M, Fan QW, et al. Expression of midkine in the early stage of carcinogenesis in human colorectal cancer. *British journal of cancer*. 1999;79(1):179-184.

61. Buck MD, O'Sullivan D, Geltink RIK, et al. Mitochondrial dynamics controls T cell fate through metabolic programming. *Cell*. 2016;166(1):63-76.

62. Dunn GP, Old LJ, Schreiber RD. The immunobiology of cancer immunosurveillance and immunoediting. *Immunity*. 2004;21(2):137-148.

63. Li C, Jiang P, Wei S, Xu X, Wang J. Regulatory T cells in tumor microenvironment: new mechanisms, potential therapeutic strategies and future prospects. *Mol Cancer*. 2020;19(1):116. doi:10.1186/s12943-020-01234-1

64. Filippou PS, Karagiannis GS, Constantinidou A. Midkine (MDK) growth factor: a key player in cancer progression and a promising therapeutic target. *Oncogene*. 2020;39(10):2040-2054.

65. Ergüven M, Muramatsu T, Bilir A. *Midkine: From Embryogenesis to Pathogenesis and Therapy*. Springer Science & Business Media; 2012. Accessed August 1, 2025. https://books.google.com/books?hl=en&lr=&id=lc8_1IAR2ZYC&oi=fnd&pg=PR5&dq=Ergu%CC%88ven+M,+Muramatsu+T,+Bilir+A.+Midkine:+from+embryogenesis+to+pathogenesis+and+therapy.

+Springer+Science+%26+Business+Media%3B+2012&ots=vHatgBCW-9&sig=8IWrtAY9jod79w-9RI-aH2wpuqc

66. Jechorek D, Haeusler-Pliske I, Meyer F, Roessner A. Diagnostic value of syndecan-4 protein expression in colorectal cancer. *Pathology-Research and Practice*. 2021;222:153431.

67. Poças J, Marques C, Gomes C, et al. Syndecan-4 is a maestro of gastric cancer cell invasion and communication that underscores poor survival. *Proc Natl Acad Sci USA*. 2023;120(20): e2214853120. doi:10.1073/pnas.2214853120

68. Yang H, Liu Y, Zhao MM, et al. Therapeutic potential of targeting membrane-spanning proteoglycan SDC4 in hepatocellular carcinoma. *Cell death & disease*. 2021;12(5):492.

69. Zhu Y, Zheng D, Lei L, et al. High expression of syndecan-4 is related to clinicopathological features and poor prognosis of pancreatic adenocarcinoma. *BMC Cancer*. 2022;22(1):1042. doi:10.1186/s12885-022-10128-y

70. Bass MD, Morgan MR, Humphries MJ. Integrins and syndecan-4 make distinct, but critical, contributions to adhesion contact formation. *Soft Matter*. 2007;3(3):372-376.

71. Becsky D, Szabo K, Gyulai-Nagy S, et al. Syndecan-4 modulates cell polarity and migration by influencing centrosome positioning and intracellular calcium distribution. *Frontiers in cell and developmental biology*. 2020;8:575227.

72. Jeyarajah MJ, Jaju Bhattad G, Kops BF, Renaud SJ. Syndecan-4 regulates extravillous trophoblast migration by coordinating protein kinase C activation. *Scientific reports*. 2019;9(1):10175.

73. Mostafavi-Pour Z, Askari JA, Parkinson SJ, Parker PJ, Ng TT, Humphries MJ. Integrin-specific signaling pathways controlling focal adhesion formation and cell migration. *The Journal of cell biology*. 2003;161(1):155-167.

74. Saoncella S, Echtermeyer F, Denhez F, et al. Syndecan-4 signals cooperatively with integrins in a Rhodependent manner in the assembly of focal adhesions and actin stress fibers. *Proc Natl Acad Sci USA*. 1999;96(6):2805-2810. doi:10.1073/pnas.96.6.2805

75. Borer RA, Lehner CF, Eppenberger HM, Nigg EA. Major nucleolar proteins shuttle between nucleus and cytoplasm. *Cell*. 1989;56(3):379-390.

76. Berger CM, Gaume X, Bouvet P. The roles of nucleolin subcellular localization in cancer. *Biochimie*. 2015;113:78-85.

Supplemental Figure 1

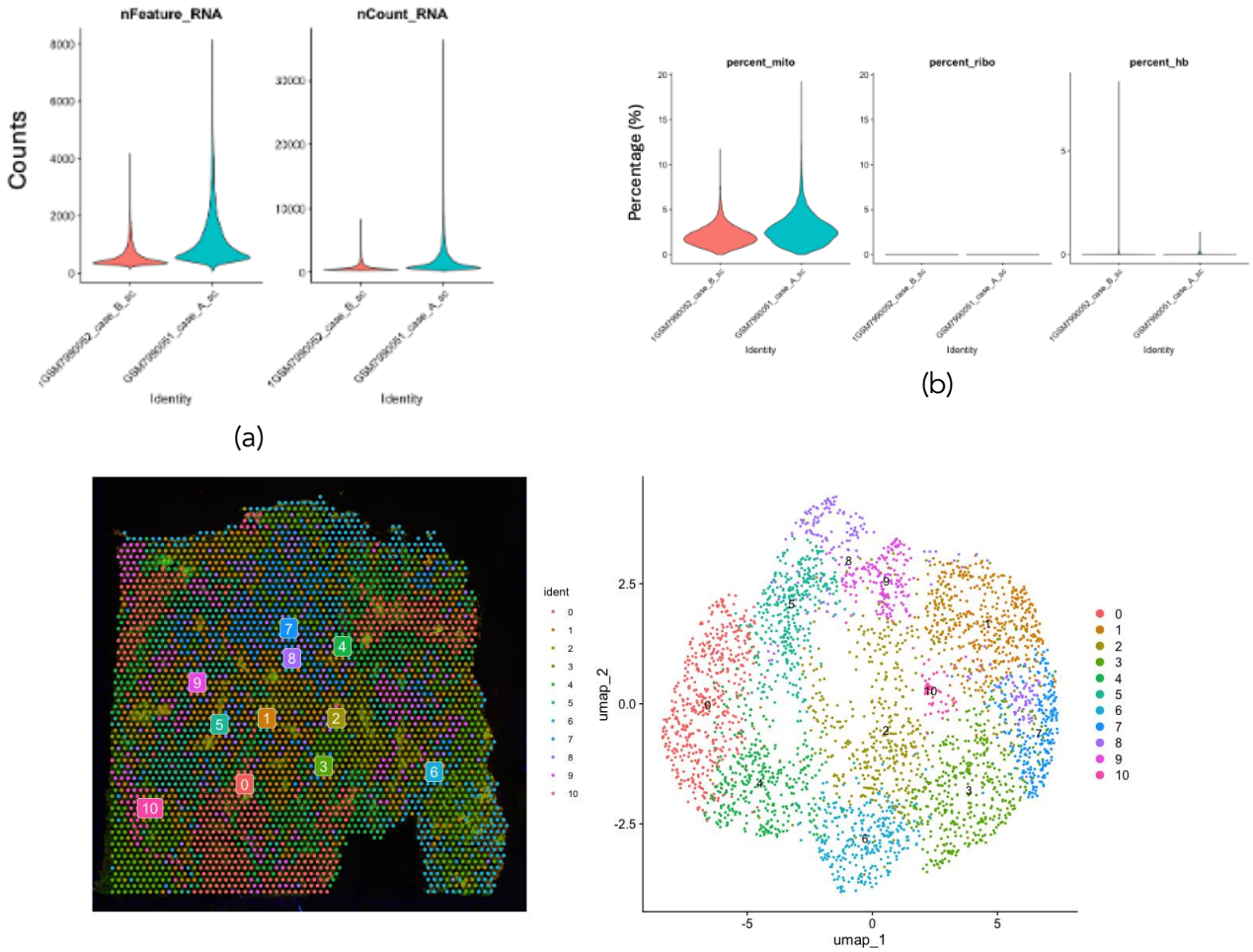

Supplemental Figure 1. The scRNA_Seq and ST data quality control: (**a**) Violin plots showing the gene (features) and mRNA counts between the anti-PD1 non-responder and responder samples after cells quality control (QC); (**b**) The percentage mitochondrial, ribosomal, or hemoglobin genes in the retained cells after QC; (**c**) Spatial clustering plot showing 11 cell clusters (left), and a Uniform Manifold Approximation and Projection (UMAP) (right);

Supplemental Figure 2

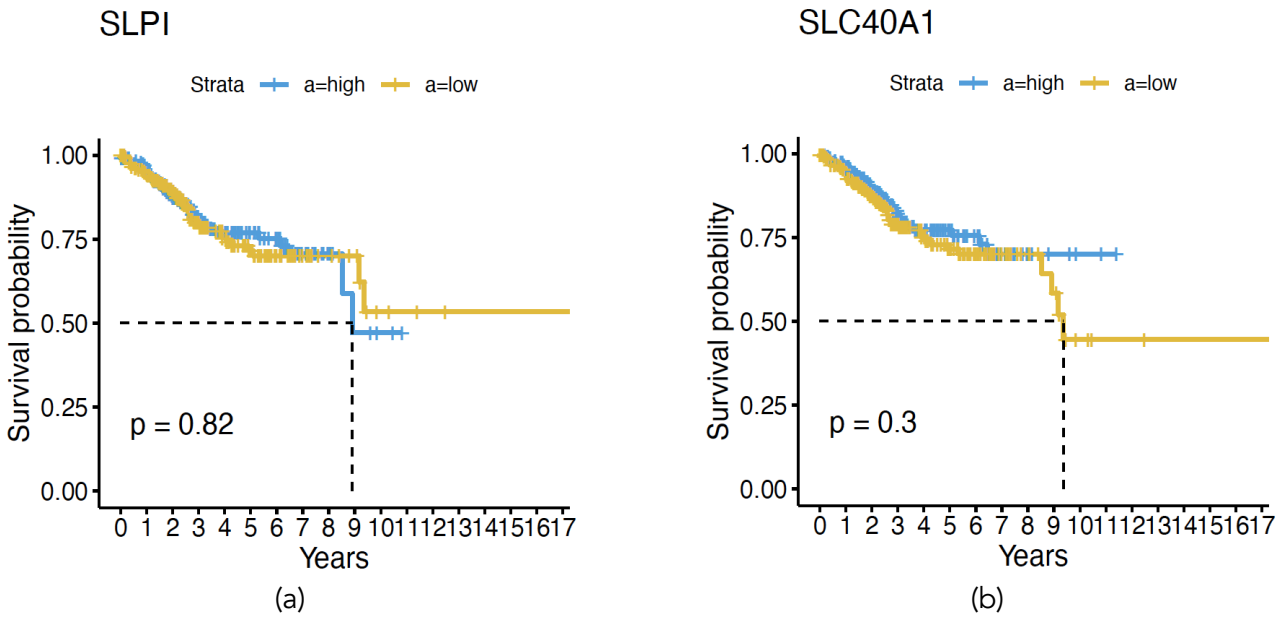

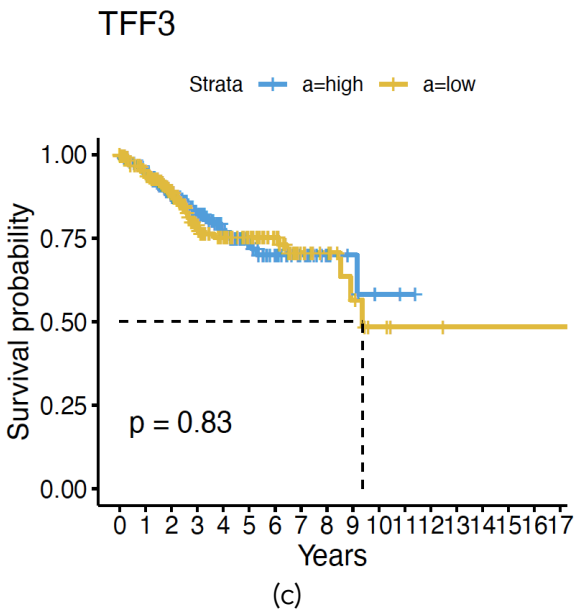

(c)

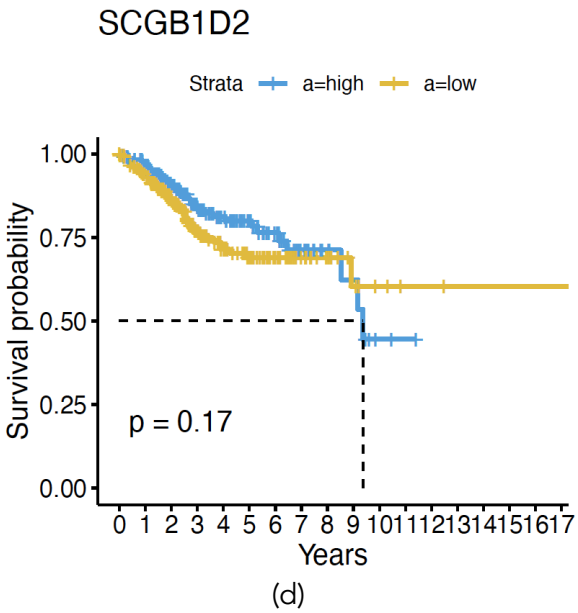

(d)

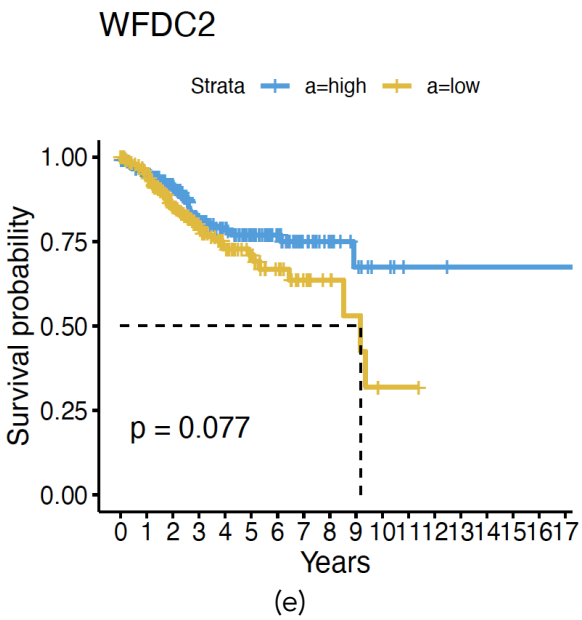

(e)

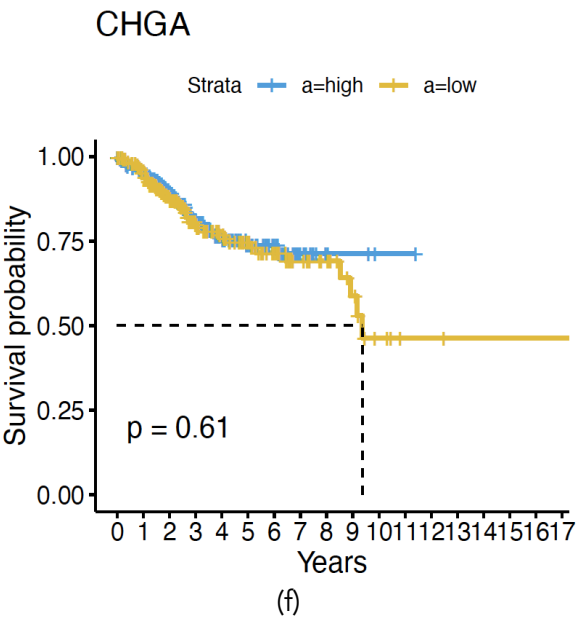

(f)

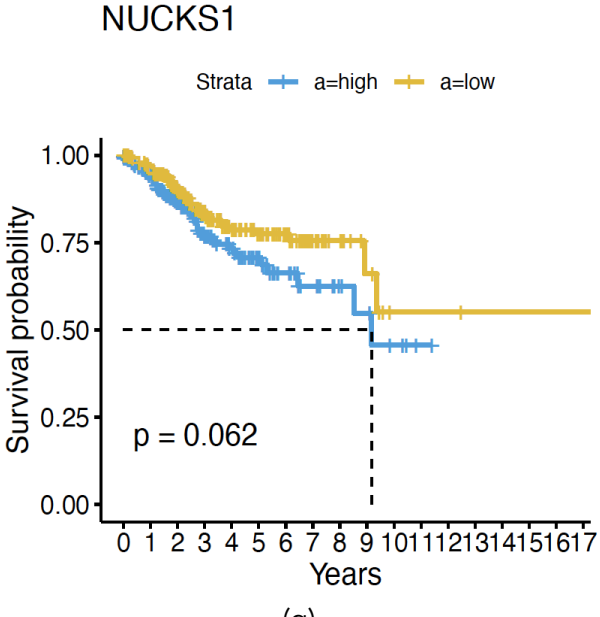

(g)

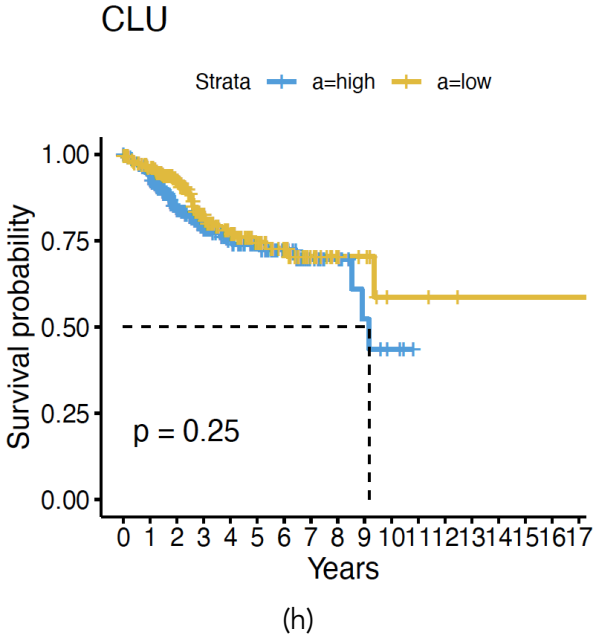

(h)

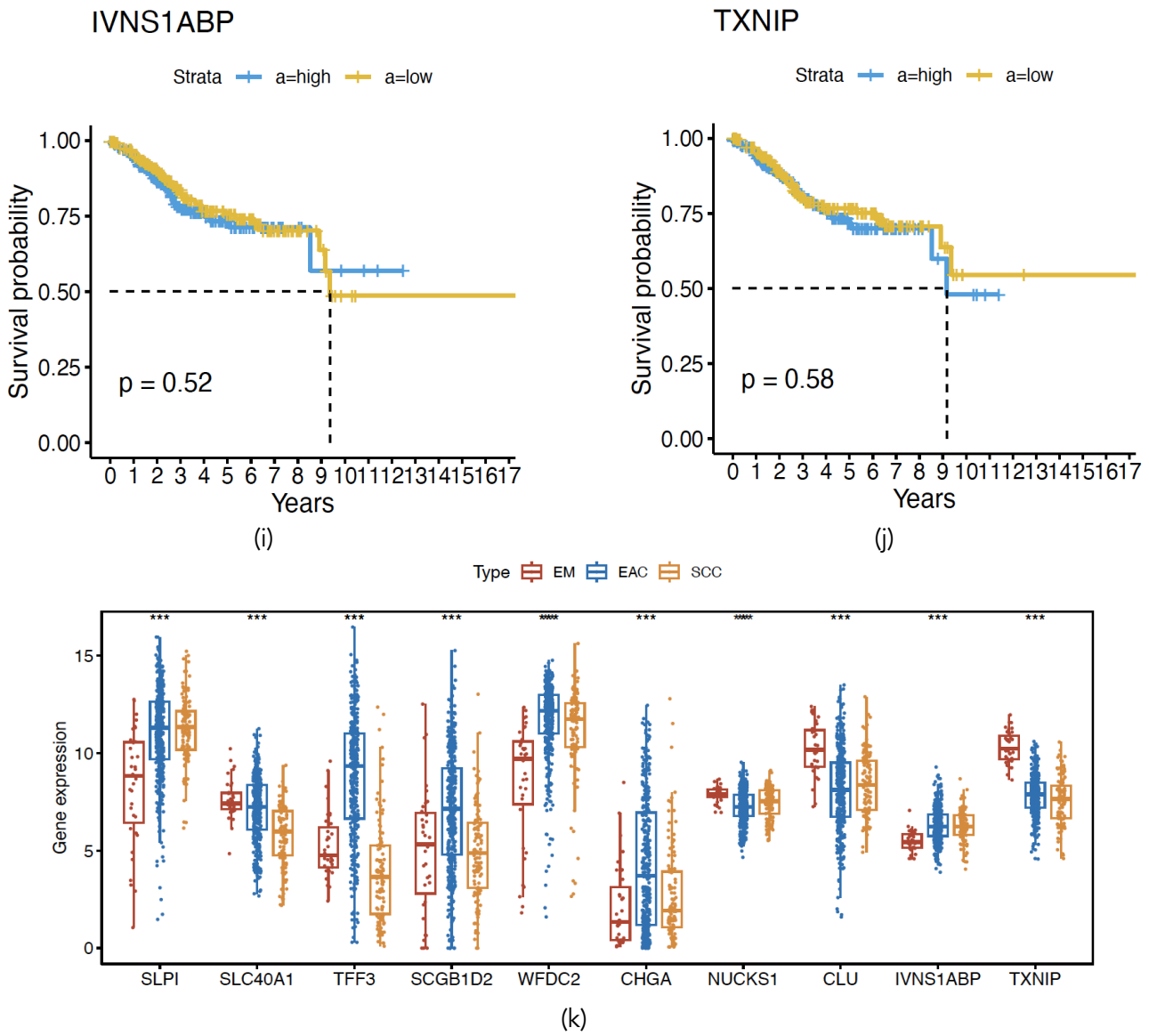

Supplemental Figure 2. DEGs predicted EC patients survival in the TCGA UCEC dataset: (**a – j**) The Kaplan-Meier plots for (**a**) SLPI; (**b**) SLC40A1; (**c**) TFF3; (**d**) SCGB1D2; (**e**) WFDC2; (**f**) CHGA; (**g**) NUCKS1; (**h**) CLU; (**i**) IVNS1ABP; and (**j**) TXNIP genes in the TCGA dataset (n = 499); (**k**) Boxplot showing expression levels of SLPI, SLC40A1, TFF3, SCGB1D2, WFDC2, CHGA, NUCKS1, CLU, IVNS1AABP and TXNIP genes in the TCGA samples from normal endometrium (EM, n = 35), endometrioid adenocarcinoma (EAC, n = 374) or serous cystadenocarcinoma (SCC, n = 125). The survival analysis was done using the suvminer and survival R packages (version 3.8-3)

Supplemental Figure 3

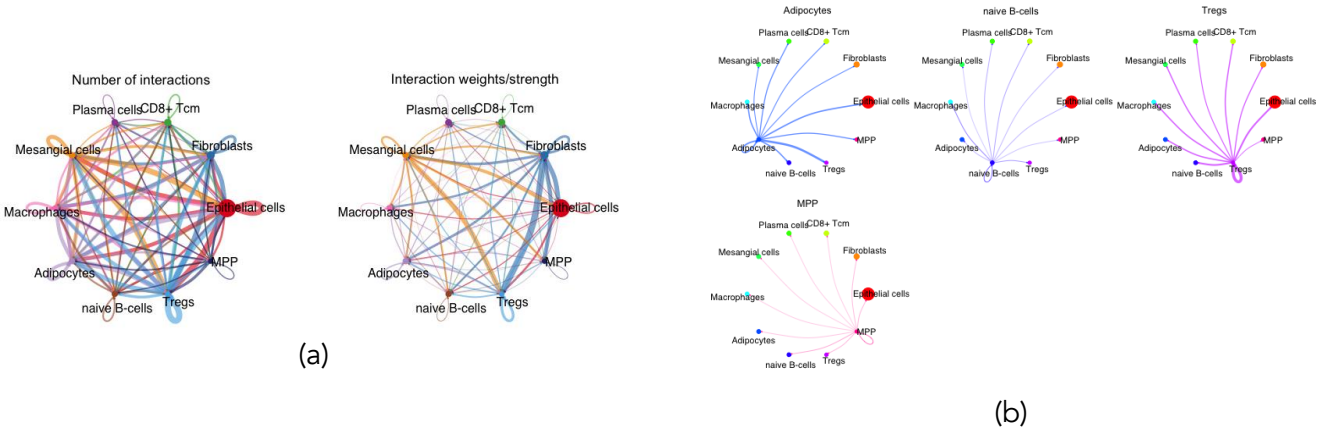

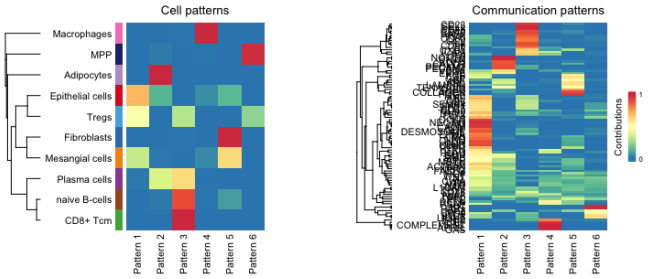
Cell patterns
Communication patterns
Macrophages
MPP
Adipocytes
Epithelial cells
Tregs
Fibroblasts
Mesangial cells
Plasma cells
naive B-cells
CD8+ Tcm
Pattern 1
Pattern 2
Pattern 3
Pattern 4
Pattern 5
Pattern 6
Contributions

(c)

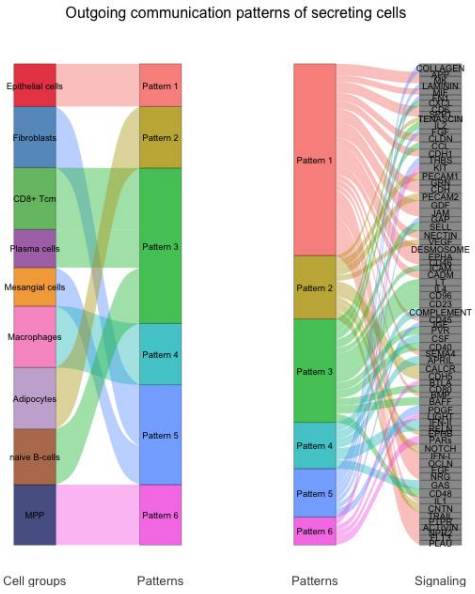
Outgoing communication patterns of secreting cells
Epithelial cells
Fibroblasts
CD8+ Tcm
Plasma cells
Mesangial cells
Macrophages
Adipocytes
naive B-cells
MPP
Pattern 1
Pattern 2
Pattern 3
Pattern 4
Pattern 5
Pattern 6
Cell groups
Patterns
Signaling

(d)

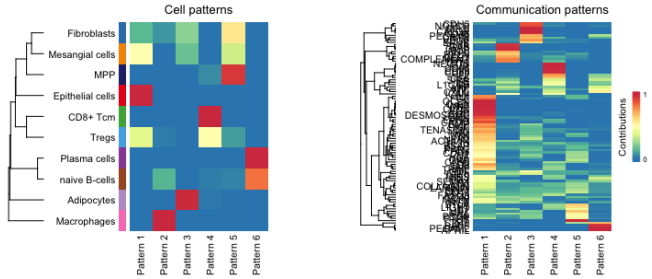
Cell patterns
Communication patterns
Fibroblasts
Mesangial cells
MPP
Epithelial cells
CD8+ Tcm
Tregs
Plasma cells
naive B-cells
Adipocytes
Macrophages
Pattern 1
Pattern 2
Pattern 3
Pattern 4
Pattern 5
Pattern 6
Contributions

(e)

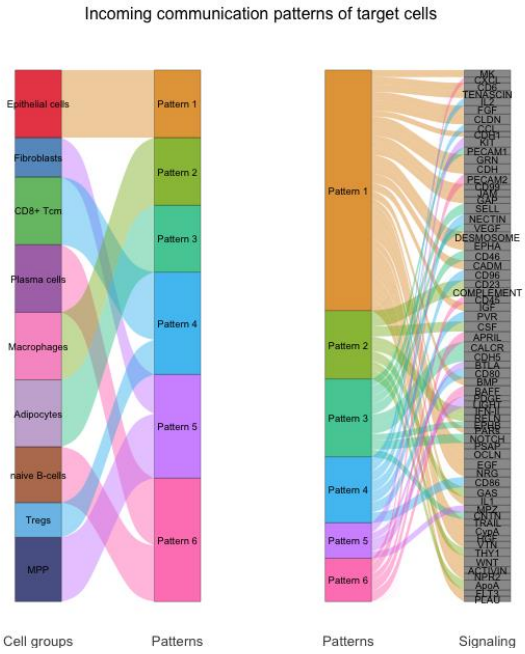
Incoming communication patterns of target cells
Epithelial cells
Fibroblasts
CD8+ Tcm
Plasma cells
Macrophages
Adipocytes
naive B-cells
Tregs
MPP
Pattern 1
Pattern 2
Pattern 3
Pattern 4
Pattern 5
Pattern 6
Cell groups
Patterns
Signaling

(f)

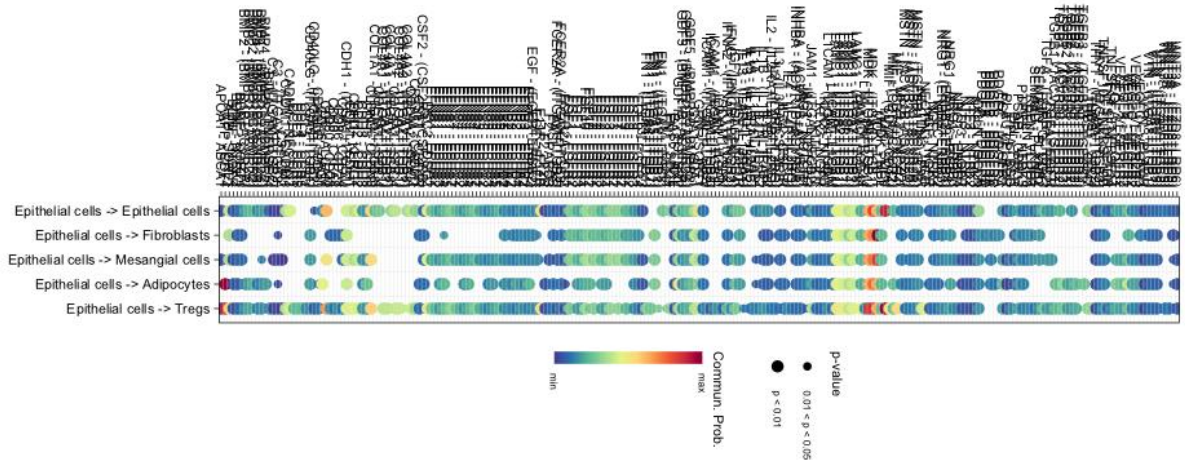
Epithelial cells -> Epithelial cells
Epithelial cells -> Fibroblasts
Epithelial cells -> Mesangial cells
Epithelial cells -> Adipocytes
Epithelial cells -> Tregs
Commun. Prob.
min
max
p-value
p < 0.01
0.01 < p < 0.05

(g)

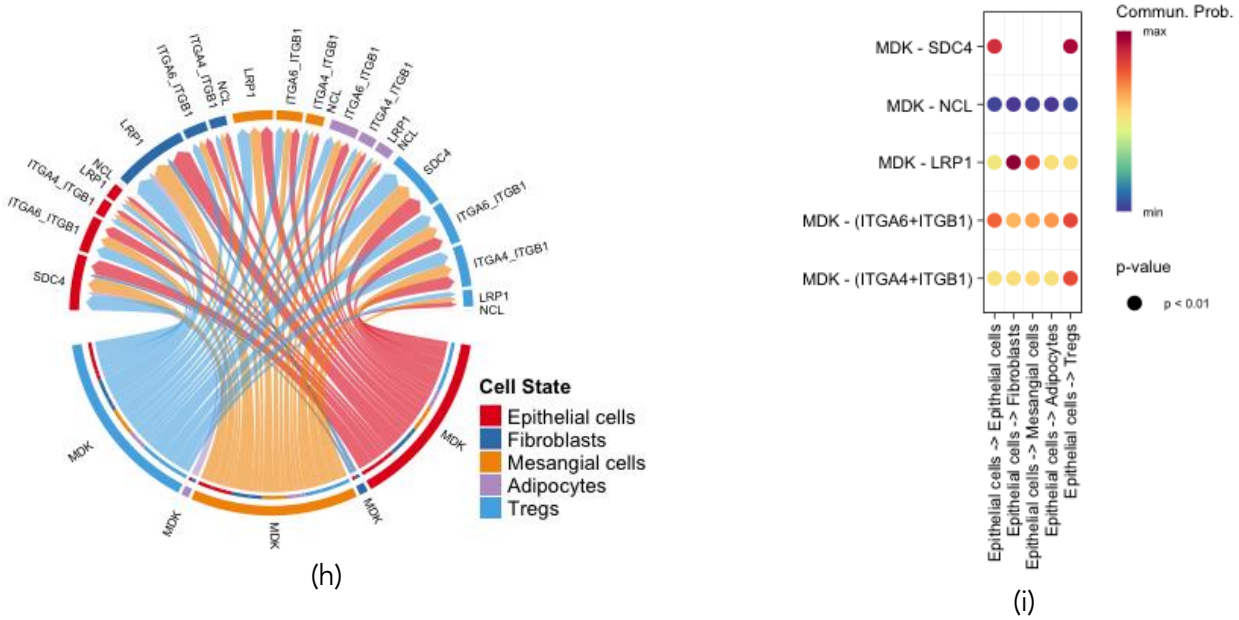

Supplemental Figure 3. Cell-cell interaction network identifies delineated overall communication patterns between anti-PD1 non-responder and responder cells: (**a**) Circle plots showing the number of interactions and the interaction strength/weights between the cells. The signal strength is denoted by the line width; (**b**) Shell diagram showing interaction between various cells. The signal strength is denoted by the line width; (**c**) Heat map showing inferred outgoing communication patterns between cells; (**d**) River plot showing inferred outgoing communication patterns between cells. The signal strength is denoted by the line width; (**e**) Heat map showing inferred incoming communication patterns between cells; (**f**) River plot showing inferred incoming communication patterns between cells. The signal strength is denoted by the line width; (**g**) The dot plot showing the contribution of all the ligand–receptor pairs in CellchatDB to signaling pathways between epithelial and epithelial, fibroblasts, mesangial, adipocytes or Tregs; (**h**) Chord plot showing inferred the MK pathway ligand-receptor signaling between epithelial and epithelial, fibroblasts, mesangial, adipocytes or Tregs. The signal strength is denoted by the line width; (**i**) The dot plot showing the comparison of the MK pathway ligand-receptor pairs contributing to the signaling between epithelial and epithelial, fibroblasts, mesangial, adipocytes, or Tregs.

Supplemental Figure 4

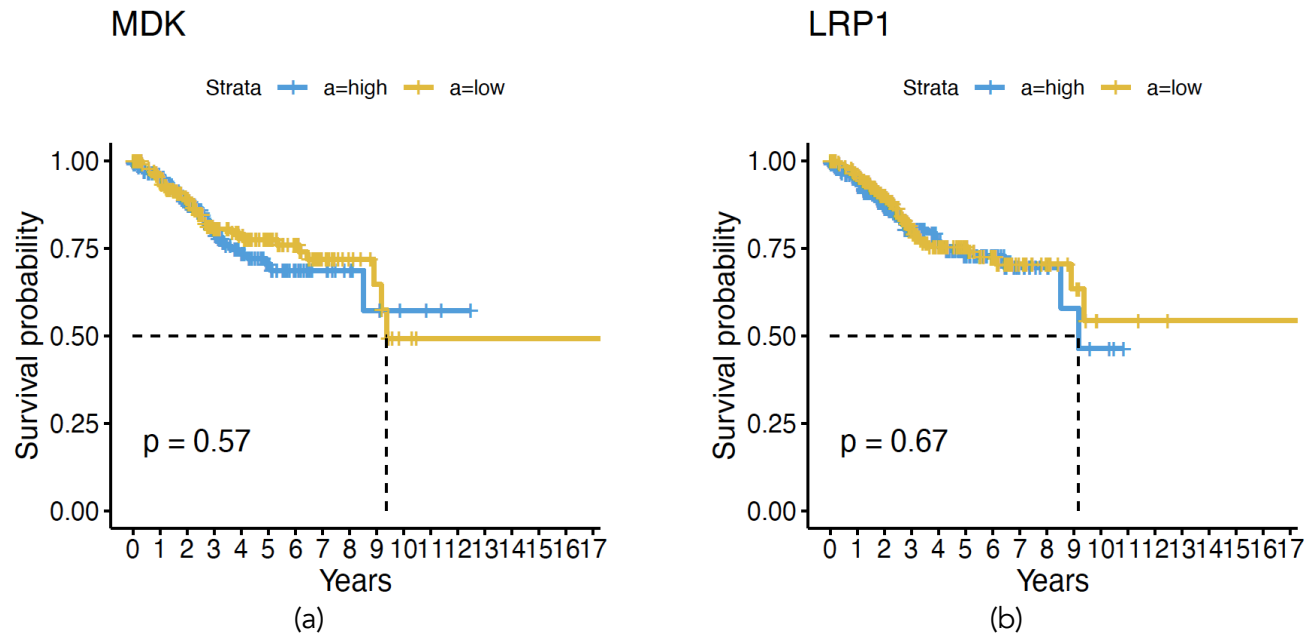

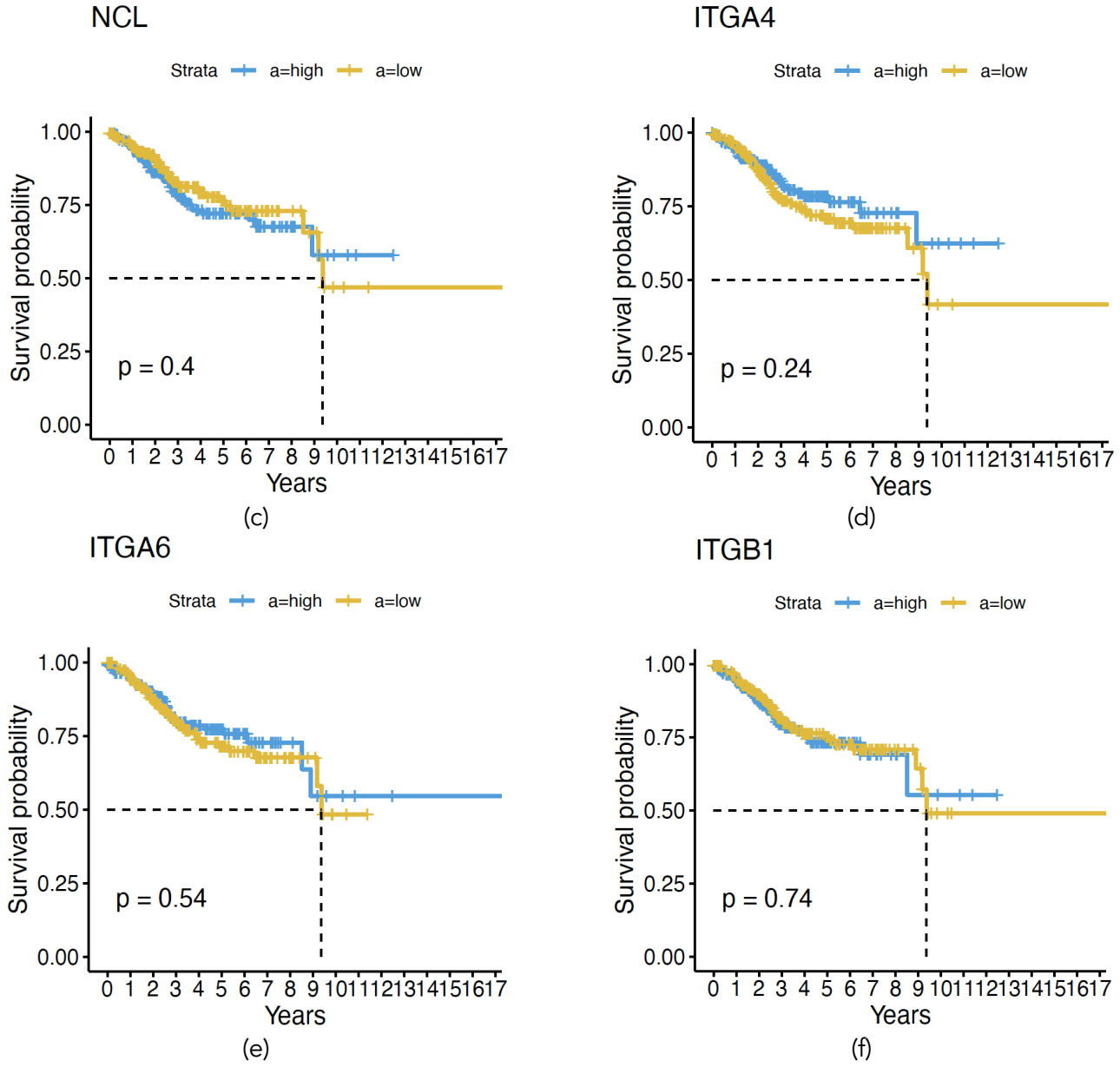

Supplemental Figure 4. Clinical significance of MDK and SDC4 expression in EC patients: (**a**) The Kaplan-Meir plots for MDK gene in the TCGA dataset (n = 499); (**b**) The Kaplan-Meir plots for LRP1 gene in the TCGA dataset (n = 499); (**c**) The Kaplan-Meir plots for NCL gene in the TCGA dataset (n = 499); (**d**) The Kaplan-Meir plots for ITGA4 gene in the TCGA dataset (n = 499); (**e**) The Kaplan-Meir plots for ITGA6 gene in the TCGA dataset (n = 499); (**f**) The Kaplan-Meir plots for ITGB1 gene in the TCGA dataset (n = 499). The survival analysis was done using the suvminer and survival R packages (version 3.8-3)

Supplemental Table 1. The anti-PD1 therapy tolerance prediction ROC scores by machine learning (ML)

		SingleR Library		
		hpca	Immu	nhd
ML Model	LASSO	0.9988819	0.9961841	0.9982478
	RIDGE	0.9982812	0.9936532	0.9965012
	ENet	0.9985092	0.9954832	0.9973745
	xgboost	0.9950883	0.9881491	0.9914755
	Linear discriminant analysis (LDA)	0.9400028	0.9416938	0.9249173
	Neural network	0.9983312	0.9964094	0.9906939
	Random forest	0.9297872	0.9361702	0.9291336
	Classification trees	0.9389654	0.9181894	0.8923237